Available online at www.sciencedirect.com
ScienceDirect
C. R. Physique 8 (2007) 1129–1150
COMPTES RENDUS PHYSIQUE
http://france.elsevier.com/direct/COMREN/

Optical parametric sources for the infrared/Sources optiques paramétriques pour l'infrarouge

Continuous-wave mid-infrared laser sources based on difference frequency generation

Weidong Chen [a,*], Julien Cousin [a], Emmanuelle Poullet [a], Jean Burie [a], Daniel Boucher [a], Xiaoming Gao [b], Markus W. Sigrist [c], Frank K. Tittel [d]

[a] *Laboratoire de physicochimie de l'atmosphère, UMR CNRS 8101, Université du Littoral Côte d'Opale 189A, Avenue Maurice Schumann, 59140 Dunkerque, France*

[b] *Anhui Institute of Optics and Fine Mechanics, Chinese Academy of Sciences, Hefei 230031, PR China*

[c] *ETH Zürich, Institute for Quantum Electronics, Laser Spectroscopy and Sensing Laboratory, Schafmattstrasse 16, CH-8093 Zürich, Switzerland*

[d] *Rice Quantum Institute, MS 366, Rice University, 6100 Main St., Houston, TX 77005, USA*

Available online 7 November 2007

Abstract

We report on recent developments of widely tunable, continuous-wave (CW) laser sources based on difference-frequency generation (DFG) in nonlinear optical materials. The state-of-the-art of CW DFG technology will be reviewed. Applications of the DFG-based laser source to high-resolution molecular spectroscopy and trace gas detection will be presented. New development trends of DFG will be discussed. ***To cite this article: W. Chen et al., C. R. Physique 8 (2007).***

Résumé

Sources lasers continues dans l'infrarouge par génération de différence de fréquences. Dans cet article nous présentons des développements récents de sources lasers, fonctionnant en régime continu et largement accordables en fréquence, basées sur la génération de différence de fréquences (DFG) lasers dans un milieu optique non linéaire. L'état de l'art de la technologie DFG sera passé en revue. Des applications de la source laser à DFG en spectroscopie moléculaire à haute résolution et à la détection de traces de gaz seront présentées. Des tendances récentes du développement de la technologie DFG seront discutées. ***Pour citer cet article : W. Chen et al., C. R. Physique 8 (2007).***

Keywords: Mid-infrared tunable laser source; Difference-frequency generation; Phase-matching; Laser absorption spectroscopy; Trace gas detection

Mots-clés : Source laser accordable dans l'infrarouge moyen ; Génération de différence de fréquences ; Accord de phase ; Spectroscopie d'absorption laser ; Détection de traces de gaz

* Corresponding author.
E-mail address: chen@univ-littoral.fr (W. Chen).

1631-0705/$ – see front matter
doi:10.1016/j.crhy.2007.09.011

1. Introduction

Developments of tunable, continuous-wave (CW) laser sources in the mid-infrared (mid-IR) spectral region from 3 to 20 μm are of considerable interest for various applications, such as:

- *Environmental applications* that include green house gas monitoring, atmospheric chemistry, fire detection, sensing of automobile, truck and aircraft exhaust emissions, combustion-generated pollutant source monitoring, catalytic converter diagnostics, and volcanic gas emissions;
- *Industrial applications* that include industrial process control, monitoring of industrial risks, fence line monitoring of industrial plants, diagnostics of gases used in the semiconductor industry;
- *Medical diagnostics applications* that include the detection, quantification and monitoring of biomarkers in exhaled breath, glucose detection, diagnostics of ulcers and colon cancer;
- *Spectroscopic applications* in high-resolution spectroscopy, reaction kinetics studies by time-resolved spectroscopy, and in studies of environment and climate relevant processes;
- *Security and military applications* that include sensing of toxic gases and biological warfare agents, detection of explosives and fugitive emissions from illicit drug-manufacturing sites, as well as infrared counter-measurements;
- *Photonic applications* that include in particular optical frequency metrology, characterization of infrared components as well as the next generation of fiber-optics communications based on novel fiber materials highly transparent in the infrared region.

Common CW sources of coherent radiation include direct laser radiation devices (denoted as class 'A' laser sources, such as color center lasers, CO and CO_2 gas lasers, interband-transition diode lasers, intraband-transition quantum cascade lasers) and devices based on nonlinear optical process (class 'B') such as difference-frequency generation and optical parametric oscillators. Currently the most useful mid-IR CW laser sources are:

- *Color center lasers (2–3.5 μm)* [1,2]: Such lasers provide an output power ranging from a few mW to several watts with a linewidth on the order of ∼MHz. Beyond its limited spectral range in the mid-infrared, a drawback is the need for liquid nitrogen cooling of the color center crystal to minimize degradation of the color center crystal and its laser performance.
- *CO (5–6 μm) and CO_2 (9–11 μm) lasers* [3,4] offer high output powers that are advantageous in highly sensitive photoacoustic spectroscopy and industrial applications, despite suffering from line-tuned spectral tunability (lasing lines are spaced by approximately 1–2 cm^{-1} in CW mode). In order to overcome the step-tunability shortcoming of the two gas lasers, the laser radiation is usually electrooptically modulated with a tunable microwave source in a CdTe or GaAs crystal to generate laser sidebands for use in spectroscopy. This technique allows ∼50% wavelength coverage within the laser lasing range. Another approach to achieve continuous tunability has been the operation at high gas pressures, as yet only in pulsed mode [5].
- *Diode lasers* [6,7]: IV–VI semiconductor lasers span the infrared wavelength range from 3 to 30 μm with an output power in the 1 mW range at cryogenical temperatures, which involves either a cryogen reservoir or a Stirling cycle cooler. As a result of over two decades of developments, distributed feedback (DFB) or distributed Bragg reflector (DBR) lasers, and external cavity diode lasers (ECDL) achieved significant progress with respect to the spectral tunability (wide tuning of ∼100 nm, and fine tuning of ∼20 cm^{-1} have been reported), as well as to the output power (CW power of ∼0.5 W has been demonstrated) [8]. Commercially available Fabry–Perot IV–VI mid-IR lasers provide single-mode injection current tuning ranges as wide as 3 cm^{-1} and individual lasers covering as much as 200 cm^{-1} of the mid-IR spectrum by varying the sink temperature from about 80 K to about 120 K [9].
- *Quantum cascade lasers (QCL)* [10–13]: Since the invention in 1994, QCLs have become one of the mid-IR laser sources of choice at specific wavelengths throughout a wide spectral region from 4 to 12 μm. QCLs exhibit high performance characteristics in terms of operating temperature, output power, and wavelength tunability. High power (10–100 mW) room temperature CW DFB-QCLs are now commercially available for specific wavelengths within the mid-IR region of 4.3–9.5 μm with a linewidth of ∼1 MHz and continuous frequency scanning by temperature tuning of ∼10 cm^{-1} [14]. Broad spectral coverage of up to 182 cm^{-1} (@ ∼ 8.4 μm) with continuous mode-hop free tuning of ∼1.25 cm^{-1} has been recently reported using a bound-to-continuum QCL design in conjunction with an external cavity grating configuration [15].

- *Interband cascade lasers (ICL)*: The concept of type-II ICLs was first proposed by Yang in 1994 [16] and demonstrated at ∼3.8 μm in quasi-CW operation in 1997. Based on interband transition (between the conduction and the valence bands) emitting 2.7 to 5.5 μm, this new class of semiconductor lasers offers low ICL threshold currents, high quantum efficiency and high output power in an important spectral region. The applicability of ICLs for trace-gas sensing has been demonstrated with cryogenically cooled ICLs. For example, the detection and quantification of H_2CO [17], as well as aircraft and balloon in situ concentration measurements of CH_4 and HCl [18] were reported recently. Development of room-temperature CW operation of ICL is in progress [19–21] and a thermoelectrically cooled CW ICL operating at 264 K was demonstrated [22].

Although these laser sources mentioned above are commercially available for the mid-IR region, each type suffers from one or more practical drawbacks: the requirement of LN_2 temperature cooling, incomplete spectral coverage or limited mode-hop free tuning range. As a viable alternative to the class 'A' infrared lasers, nonlinear optical frequency down-conversion can be employed to generate class 'B' optical parametric sources, based on optical parametric oscillators or difference-frequency generation. As a result of the development of high-power tunable near infrared laser pump sources in combination with quasi-phase-matching nonlinear optical materials with high nonlinear conversion efficiency and high damage threshold, CW optical parametric laser sources have been configured as stable coherent sources broadly tunable in the mid-IR region, which allow the transfer of the high performance characteristics of the pump lasers to the mid-IR: precise wavelength resolution, narrow linewidths, widely and rapidly continuous wavelength tunability.

- *Optical parametric oscillators (OPO)*: CW optical parametric oscillators operate as tunable mid-infrared spectroscopic sources up to ∼4.5 μm with narrow-linewidth (<MHz), high power (∼W) and smooth, mode-hop-free tuning up to 60 GHz [23–25]. Continuous mode-hop free frequency tuning across the coarse frequency tuning region with active stabilization of the laser frequency and the cavity lengths have been reported by Harren [26–28] and Henderson [29].
- *Difference-frequency generation (DFG)*: Laser sources based on CW DFG in a suitable nonlinear optical material offer a spectroscopic source capable of precise wavelength resolution, narrow linewidth, widely and rapidly continuous wavelength tunability. The first continuous-wave DFG source was reported by Pine [30] in 1974 for use in high-resolution spectroscopy in the infrared (2.2–4.2 μm) by mixing a single mode Ar^+ laser with a single frequency CW dye laser in a 5-cm long $LiNbO_3$ crystal. Extension of the infrared spectral coverage to the mid- and long-wave infrared using DFG was initially limited by the availability of effective pump lasers and suitable nonlinear optical materials in the 1970s and 1980s. Experiments of DFG-based infrared sources from 4 to 10 μm by the Laser Science Group at Rice University (Houston) in 1991 [31,32] represent an important milestone in the modern development of DFG-based CW laser sources. Wide wavelength tuning was achieved by mixing a dye and a Ti:Sapphire laser in an $AgGaS_2$ crystal. Since then, there has been a renaissance in DFG technology as a result of significant advances in nonlinear optical materials, pumping lasers and photonics technology [33,34].

In this article we emphasize mid-IR laser sources based on CW difference-frequency generation. Several reviews of DFG-based laser sources have been published (e.g. Refs. [35–38]). The scope of this paper is to discuss recent progress in the developments of CW DFG in the mid-infrared with emphasis on phase-matchable nonlinear optical materials, phase-matching schemes, laser pumping sources, DFG in the deep infrared and power conversion efficiency. Typical applications of coherent sources based on nonlinear optical frequency-conversion to spectroscopic applications will be presented.

2. Difference-frequency generation

Difference-frequency generation as a three-wave nonlinear interaction process has been theoretically analyzed by Armstrong et al. [39] in 1962. The difference-frequency conversion efficiency has been investigated by Boyd and Kleinman [40], based on the electric field generated by two focused Gaussian beams, the dependence of the generation power on the focusing condition and the properties of the nonlinear mixing material. In the case of two collinear Gaussian beams (with powers P_p and P_s at frequencies ω_p and ω_s, for the pump and signal beam, respectively)

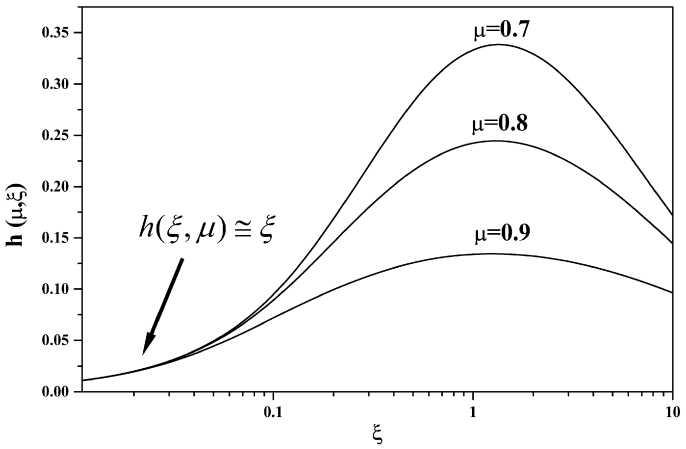

Fig. 1. Relative DFG conversion efficiency (h-function) using focused Gaussian beams [40]. Where $h(\mu, \xi, \alpha)$ is the focusing function (Eq. (2)), $\mu = k_p/k_s$ and $\xi = L/b$ is the focusing parameter.

having identical confocal parameters $b = k_p w_p^2 = k_s w_s^2$ (here w is the beam waist), the DFG output power P_i, at the difference-frequency ω_i ($= \omega_p - \omega_s$), can be written as [41,42]:

$$P_i = \frac{256\pi^2}{c^3} \cdot \omega_i \cdot \frac{(d_{\text{eff}})^2}{n_i \cdot n_s \cdot n_p} \cdot \frac{h(\mu, \xi, \alpha)}{(k_s^{-1} + k_p^{-1})} \cdot L \cdot P_p \cdot P_s \cdot \exp(-\alpha L) \tag{1}$$

here c is the speed of light in vacuum, n is the index of refraction, L is the crystal length, d_{eff} is the effective nonlinear coefficient, and α is the absorption coefficient of the nonlinear optical medium at the DFG frequency. The subscripts s, p, i refer to the signal, pump, and idler (infrared), respectively. The focusing function $h(\mu, \xi, \alpha)$ involving walk-off and focused beam effects is given as (focusing point is assumed at the center of the crystal):

$$h(\mu, \xi, \alpha) = \frac{1}{4 \cdot \xi} \cdot \int_{-\xi}^{+\xi} \mathrm{d}\tau \cdot \int_{-\xi}^{+\xi} \mathrm{d}\tau' \cdot \frac{\exp(\frac{b \cdot \alpha}{4}(\tau - \tau'))}{1 - \frac{j}{2} \cdot (\frac{1+\mu}{1-\mu} + \frac{1-\mu}{1+\mu}) \cdot (\tau - \tau') + \tau \cdot \tau'} \tag{2}$$

where $\mu = k_p/k_s$ and the focusing parameter $\xi = L/b$ which relates the crystal length to the beam size of the pump and signal. Fig. 1 plots the focusing function h versus the focusing parameter ξ.

Eq. (1) shows typical features for a three-wave parametric mixing process:

1. DFG power is proportional to the nonlinear optical figure of merit, $d_{\text{eff}}^2/(n_i n_s n_p)$.
2. The output power varies linearly with the product of the input powers. In practice, the pumping power densities incident on the nonlinear optical crystal are usually limited by the laser induced damage of the crystal. A large optical damage threshold is thus highly desirable. Commercially available ferroelectric material-based quasi-phase-matching (QPM) crystals, such as periodically poled $LiNbO_3$ (PPLN) or $RbTiOAsO_4$ (PPRTA), exhibit high laser induced damage thresholds and lead to mW CW DFG power by using high-power (∼W) pumping sources. In the case of using low pumping powers, intracavity DFG technique [43–45], semiconductor optical amplifiers or fiber amplifiers [46] can be used to enhance pumping power levels.
3. DFG power is proportional to the square of infrared frequency ω_i, as shown in Fig. 2.
4. As shown in Fig. 1, the DFG power varies with the crystal length L in the case of Gaussian beam coupling, and reaches a maximum value with an optimum focusing parameter of $\xi \sim 1.3$. The h-function reduces to $h \sim \xi$ when using loose focusing parameter $\xi \ll 1$, which makes the DFG power proportional to L^2, as in the case of the plane-wave approximation where the nonlinear generation power at the resultant frequency ω_i can be written as:

$$P_i \propto \frac{d_{\text{eff}}^2}{n_i \cdot n_p \cdot n_s} \cdot \omega_i^2 \cdot P_p \cdot P_s \cdot L^2 \cdot \sin c^2\left(\frac{|\Delta k| L}{2}\right) \cdot \exp(-\alpha L) \tag{3}$$

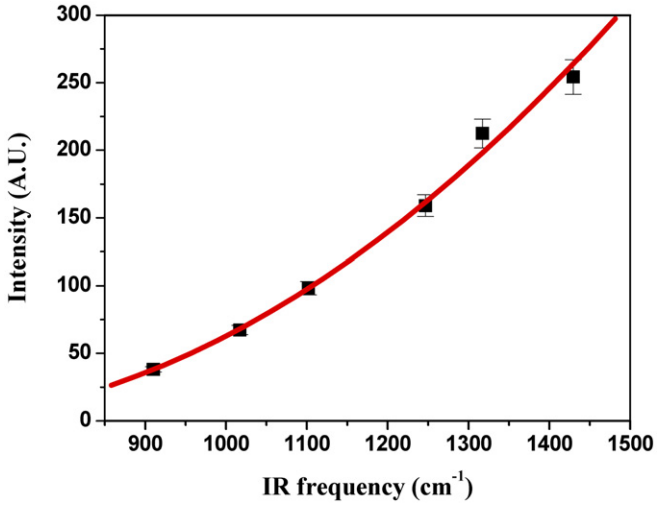

Fig. 2. Output power versus infrared frequency of 900–1500 cm^{-1} (6.6–11.1 μm) from type II phase-matched (see Section 3.1). DFG in a $LiInS_2$ crystal in the X–Y plane. Squares, experimental data; solid curve, quadratic fit [48].

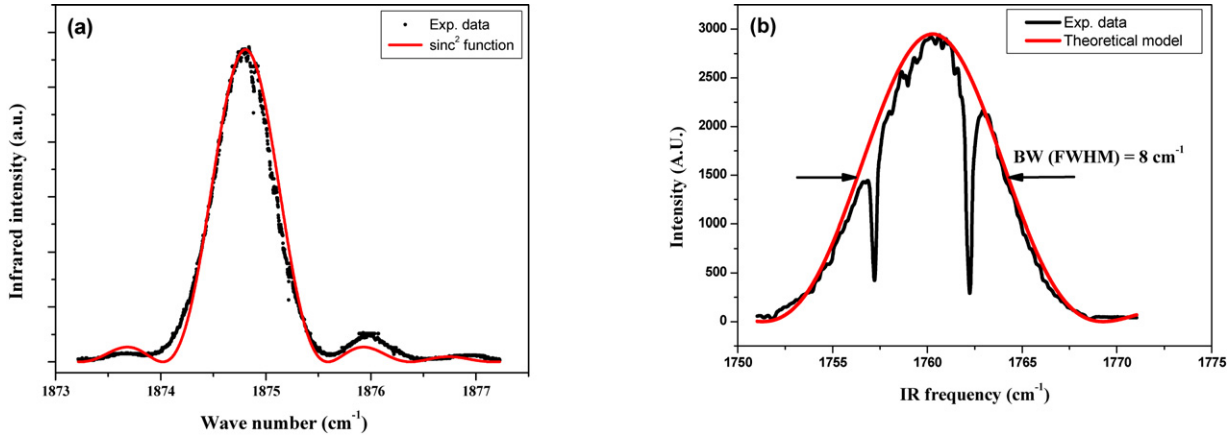

Fig. 3. DFG infrared frequency detuning characteristics at room temperature: (a) in a 45-mm long $AgGaS_2$ crystal [47]; (b) in a 10-mm long $LiInS_2$ crystal [48]. Black: experimental data; Red (lighter line): $sinc^2$ function that considers phase mismatch in the frequency-conversion process, based on a plane-wave model. The asymmetry of the experimental curve is due to interaction effects of focused Gaussian beams [41,42]. The observed phase-matched wavelength-tuning bandwidth (FWHM) was 0.6 cm^{-1} for $AgGaS_2$ and 8 cm^{-1} for $LiInS_2$, respectively. In (b), two atmospheric water-vapor absorption lines (010–000) were observed in laboratory ambient air over a 42.5-cm open path between the DFG crystal and the MCT detector. (For interpretation of the references to color in this figure legend, the reader is referred to the web version of this article.)

where $\mathbf{k}$ is the wave vector within the nonlinear optical medium and $\Delta\mathbf{k}$ $(= \mathbf{k}_p - \mathbf{k}_s - \mathbf{k}_i)$ describes the phase mismatch resulting from unequal phase velocities of the interacting waves. In fact, due to optical frequency dispersion in the refractive index of nonlinear optical crystals, the interacting waves at different frequencies travel at different velocities (defined as $c/n(\omega)$, where $n(\omega)$ is the frequency-dependent refractive index). The difference in the phase velocities produces a phase difference that accumulates along the length of the nonlinear device. The relative phases of the interacting waves determine the direction of the power flow between the driving and generated waves. A phase shift of π is produced in every coherence length ($L_c = \pi/\Delta k$), which leads to a reversal of the energy flow from the generated wave to the driving waves. For efficient frequency-conversion, a critical requirement is that the interacting waves must stay in phase along their path through the nonlinear optical medium. This requirement is usually referred to as phase-matching (PM) [39]. Maximum frequency-conversion efficiency can be obtained when the phases of the interacting waves are matched so that $\Delta\mathbf{k} = 0$. Fig. 3 depicts the phase-mismatching effect of the DFG process: (a) in a 45-mm long $AgGaS_2$ crystal [47]; (b) in a 10-mm long $LiInS_2$ crystal [48]. The asymmetry of the experimental curve is due to interaction effect of focused Gaussian beams [41,42].

In the case of a collinear interaction, the PM condition can be expressed as:

$$\frac{n_i}{\lambda_i} = \frac{n_p}{\lambda_p} - \frac{n_s}{\lambda_s} \tag{4}$$

where

$$\frac{1}{\lambda_i} = \frac{1}{\lambda_p} - \frac{1}{\lambda_s}$$

The refractive indices can be calculated by using a wavelength-dependent dispersion equation, known as the Sellmeier equation, and given as:

$$n^2(\lambda) = A + \frac{B}{1-(C/\lambda)^2} + \frac{D}{1-(E/\lambda)^2} \tag{5}$$

where the dispersion coefficients A, B, C, D, E for most of the commercially available materials are reported in Refs. [49,50].

3. State of the art of CW DFG technology

3.1. Phase-matching methods

3.1.1. Birefringent phase-matching (BPM)

This method is used for semiconductor materials such as uniaxial crystals: $AgGaS_2$, $AgGaSe_2$, GaSe, $ZnGeP_2$ or biaxial crystals: $LiInS_2$, $LiInSe_2$. In the BPM scheme, birefringence is used to adjust the different phase velocities by matching the field polarizations of the different mixing waves to the phase-matching required crystal axis (if the signal and idler have the same polarization, this type of phase matching is referred to *type I* PM; while the case of different polarizations for the signal and idler corresponds to a *type II* interaction). For this purpose orthogonal polarizations between interacting waves are required with an appropriate combination of the pump and signal wavelengths. For instance, type I BPM of a 3-wave collinear interaction can be written as:

$$\frac{n_o(T,\lambda_i)}{\lambda_i} = \frac{n_e(\theta,T,\lambda_p)}{\lambda_p} - \frac{n_o(T,\lambda_s)}{\lambda_s} \tag{6}$$

Eq. (6) can be satisfied by adjusting the pumping wavelengths, the crystal temperature, and the incident angle of the pumping beams with respect to the optic axis of the nonlinear optical crystal.

- *Wavelength tuning*: The wavelengths of the pump and signal lasers are selected so that the wavelength-dependent refractive indices at each of the three interacting frequencies are phase-matched. This implies that their respective polarizations should be phase-matched as required by the crystal orientation.
- *Temperature tuning*: PM can be obtained by adjusting the temperature-dependent refractive indices. This technique is useful when the birefringence of the crystal is strongly sensitive to temperature and if fast tuning is not required.
- *Angle tuning*: The refractive indices can be varied by angular orientation of the crystal optic axis with respect to the propagation direction of the incident pump laser beams. This method, however, may introduce 'walk-off' effects of the Poynting vector for the extraordinary wave due to double refraction. This effect leads to a reduction of the spatial overlap between the interacting waves, and thus degrades the parametric conversion efficiency.

In general, one technique can be used in combination with another to achieve phase-matched DFG over a wide spectral region. Fig. 4 shows a typical example of BPM using wavelength tuning in conjunction with angle orientation to cover the mid-IR region from 8 to 19 μm by DFG in a GaSe crystal [51,52].

Phase-matching using birefringence requires finding a coincidence between the birefringence-dependent wavelengths of interest and those available from pump sources which satisfies $\Delta k = 0$ and fall within the optical transmission range for a given crystal. This requirement restricts the number of crystals suitable for nonlinear frequency-conversion to only about ten commercially available crystals for infrared DFG applications [49]. The typical power conversion efficiency is $\sim 10^{-5}/(\mathrm{W\,cm})$.

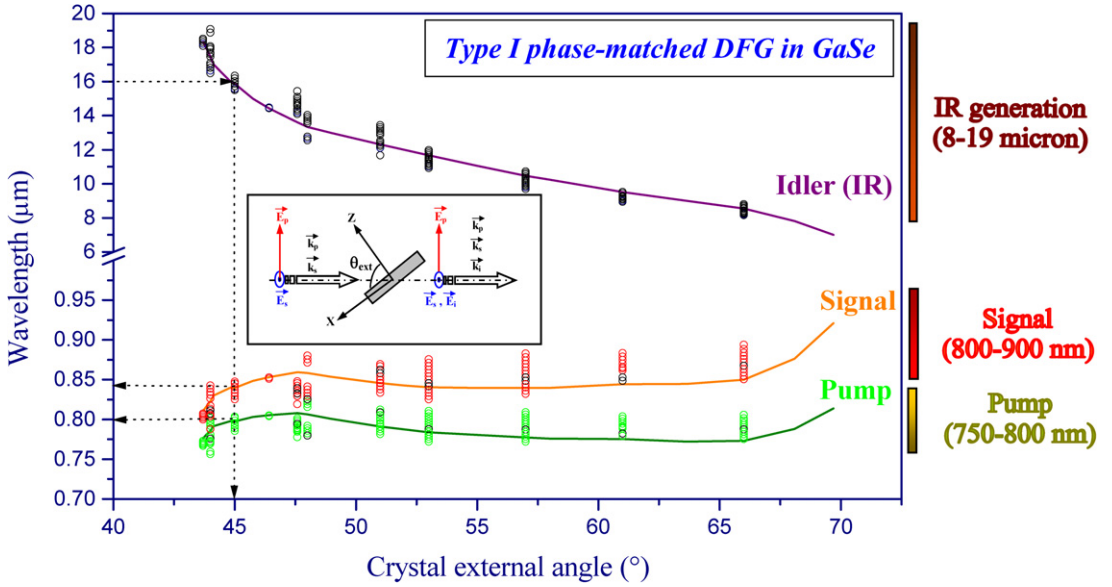

Fig. 4. Infrared wavelength tuning characteristics of DFG in a GaSe crystal from 8 to 19 μm, birefringently phase-matched by tuning of laser wavelengths and crystal angle. The solid curves are calculated based on the Sellmeier equation given in [169] and the dots correspond to experimental data [52].

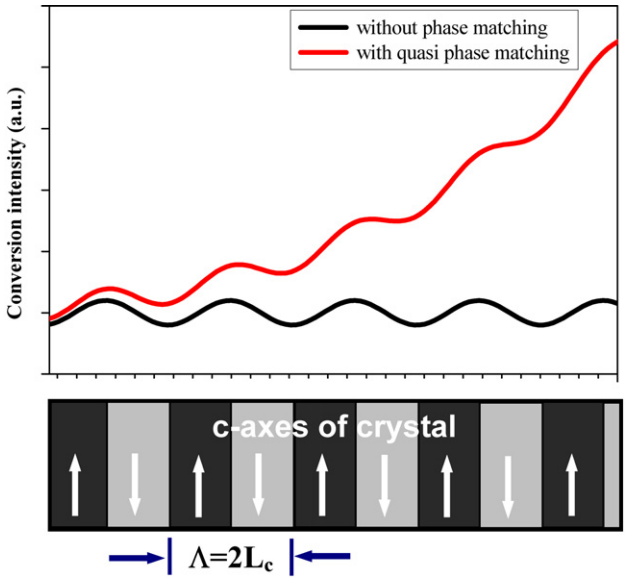

Fig. 5. Quasi-phase-matching scheme using a periodical structure to offset the accumulated phase mismatch along the propagation direction of the interacting waves in a nonlinear optical crystal.

3.1.2. Quasi-phase-matching (QPM)

In a QPM scheme, periodic structures are used to offset the accumulated phase mismatch: the signs of the optical nonlinearity of the crystals are modulated along the propagation direction so that the phase is periodically reset by π with a half-period equal to the coherence length L_c as illustrated in Fig. 5.

The modulation period $\Lambda = 2L_c$ should be appropriately selected so that the following QPM equation is satisfied:

$$\frac{n(T,\lambda_i)}{\lambda_i} = \frac{n(T,\lambda_p)}{\lambda_p} - \frac{n(T,\lambda_s)}{\lambda_s} - \frac{1}{\Lambda} \tag{7}$$

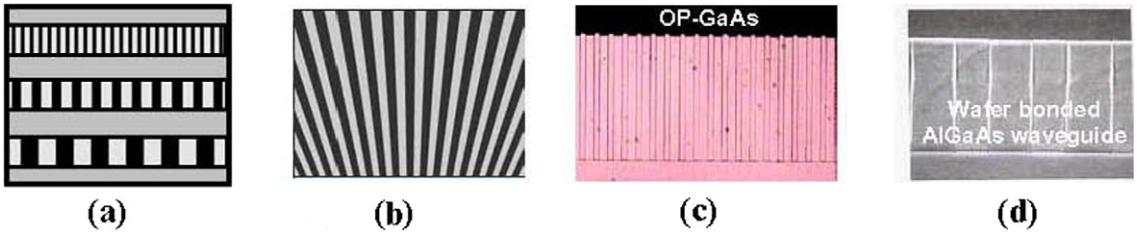

Fig. 6. Various grating designs for electric-field poling of ferroelectric materials: (a) multiple channels [56], (b) fan-out grating [58]. QPM semiconductors: (c) epitaxial orientation patterned growth GaAs [62] and (d) wafer bonded AlGaAs waveguide [77].

In contrast to BPM, the QPM materials can be engineered to be phase-matchable at any wavelengths within the transparency range of the crystal by selecting the appropriate modulation period Λ. This method allows a free choice of polarization of the interacting waves and the use of the largest nonlinear susceptibility component. Moreover, as the QPM scheme does not rely on birefringence, it can be used in isotropic materials with a large optical nonlinearity. Three techniques have been implemented to realize QPM in bulk materials or waveguided QPM:

(1) Photolithographically patterning method [53–55], used for electric-field poling of ferroelectric materials (such as $LiNbO_3$, $KTiOPO_4$, $RbTiOAsO_4$, $LiTaO_3$, $KTiOAsO_4$) to provide precise periodical domain sizes ranging from 5 to 30 μm. When Λ is appreciatively selected, DFG frequency tuning can be realized by adjusting temperature and/or angle between the crystal optic axis and the propagation direction of the incident laser beams. In order to realize wide frequency tunability, a multi-grating design is employed (Fig. 6(a)) [56,57]. A fan-out grating design can be used for a continuously and widely tunable optical parametric source (Fig. 6(b)) [58]. An angled and staggered grating used for QPM of the antisymmetric TM_{10} mode in PPLN has been demonstrated by Fejer et al. [59].
(2) Epitaxial orientation patterned growth [60–62] (Fig. 6(c)) or (3) diffusion stacking–bonding [63–69] (Fig. 6(d)) methods, applied to III–V semiconductors (such as GaAs, ZnSe).

3.1.3. Waveguide phase-matching

The efficiency of traveling-wave bulk interactions is restricted by a trade-off between tight focusing for high laser intensities and loose focusing for large interaction lengths. Waveguide devices offer interacting guided waves inside nonlinear optical media, which minimizes diffraction effects and yields potentially single-pass frequency-conversion efficiencies that are two or three orders of magnitude (up to 19% W^{-1} [70]) larger than that obtained with single-pass interaction in a bulk crystal. Waveguide PM devices can be classed as follows:

(1) Dielectric waveguided QPM nonlinear materials, such as waveguided PPLN [71–73] and recently reported direct-bonded QPM PPLN ridge waveguides [74,70,75].
(2) Waveguided semiconductors (like GaAs, ZnSe) using QPM based on periodic domain inversion by wafer bonding [76,77].
(3) Modal dispersion PM based on engineered birefringence (form birefringence PM) in oxidized GaAs–AlAs multiplayer waveguide [78–80].
(4) Total internal reflection-based Zig-Zag Fresnel QPM in isotropic semiconductors [81–84].

A new approach, named random phase-matching, has been recently proposed. This approach is based on the random motion of the relative phases in highly transparent polycrystalline materials to achieve efficient phase matching in isotropic materials [85]. A recent review of quasi-phase-matching technology can be found in Refs. [86,87].

3.2. Phase-matchable materials

Requirements for nonlinear optical materials for effective frequency-down conversion include: optical transparency at the three frequencies of the interacting waves, phase matchable with a nonlinear coefficient $\chi^{(2)}$ as large as possible

Table 1
Properties of some important phase-matchable nonlinear optical materials suitable for mid-IR DFG applications [50], and (a): [127], (b): [170], (c): [171], (d): [172], (e): [173], (f): [123]

Crystal	Abs. coef. (cm^{-1})	Transparency (μm)	Nonlinear coefficient (pm/V)	Damage threshold (MW/cm^2)
$KTiOPO_4$	<0.01 (@1.06 μm)	0.35–4.5	$d_{33} = 10.7$ (@ 1.064 μm)	150 (@1.064 μm & 20 ns)
$KTiOAsO_4$	<0.005 (@1.06 μm)	0.35–5.3	$d_{33} = 16.2$ (@ 1.064 μm)	400 (@1.064 μm & 10 ns)
$LiNbO_3$	0.002 (@1.06 μm)	0.4–5.5	$d_{33} = -27$ (@ 1.06 μm)	100 (@1.064 μm & 20 ns)
$RbTiOAsO_4$	<0.005 (@1.06 μm)	0.35–5.8	$d_{33} = 15.8$ (@ 1.064 μm)	400 (@1.064 μm & 10 ns)
$LiIO_3$	0.2 (@1.06 μm)	0.28–6	$d_{33} = 4.5$ (@ 1.064 μm)	120 (@1.064 μm & 10 ns)
$LiInS_2$[(a)]	<0.04 (@1.06 μm)	0.34–11.5	$d_{33} = 16$ (@ 2.3 μm)	1000 (@1.06 μm & 10 ns)
$LiInSe_2$	<0.06 (@1.06 μm)[(b)]	0.5–12.5	$d_{\text{eff}} = 11$ (@ 7 μm)[(c)]	500 (@1.06 μm & 10 ns)
$ZnGeP_2$	0.03 (@4.5–8 μm)	0.74–12	$d_{36} = 68.9$ (@ 10.6 μm)	78 (@9.6 μm & 120 ns)
$AgGaS_2$	<0.04 (@4–8.5 μm)	0.47–13	$d_{36} = 11.1$ (@ 10.6 μm)	20 (@10.6 μm & 150 ns)
GaAs	0.01 (@10 μm)	0.9–17	$d_{14} = 94$[(d)], $d_{36} = 119$[(e)]	
$CdGeAs_2$	0.4 (@10.6 μm)	2.4–18	$d_{36} = 282$ (@ 10.6 μm)	33 (@10.6 μm & 150 ns)
$AgGaSe_2$	0.09 (@10.6 μm)	0.71–19	$d_{36} = 33$ (@ 10.6 μm)	15 (@10.6 μm & 150 ns)
GaSe	<0.1 (@10.6 μm)	0.62–20	$d_{22} = 54$ (@ 10.6 μm)	30 (@10.6 μm & 125 ns)
ZnSe	<0.005 (@10 μm)	0.5–22	$d_{14} = 78$ (@ 10.6 μm)[(f)]	
CdSe	0.03 (@10.6 μm)	0.75–25	$d_{31} = -18$ (@ 10.6 μm)	60 (@10.6 μm & 200 ns)

and a high optical damage threshold. Also important are optical homogeneity, mechanical, thermal properties and commercial availability.

Table 1 lists the principal nonlinear optical media currently used for DFG applications in the 3 to 20 μm region. A good review of nonlinear materials for optical frequency-conversion can be found in Refs. [88,89,55,38].

As can be seen, ferroelectric materials exhibit a larger damage threshold although they are optically transparent to only ∼5 μm due to intrinsic absorption, while semiconductors materials are suitable for DFG in the deep mid-IR at wavelength $\lambda > 5$ μm. Ferroelectric material-based QPM crystals are commercially available, while commercialisation of OP-GaAs materials is currently in progress.

3.3. Practical laser pump sources suitable for CW DFG based mid-infrared sources

The spectral features of a DFG coherent light source are determined by the characteristics of the pump lasers selected for a particular source platform. Hence the following parameters for laser sources are desirable: (1) narrow pump laser linewidths, preferably single longitudinal mode (since the DFG emission linewidth is equal to the convolution of the pump laser linewidths under Gaussian beam profile assumption); (2) wavelength tunability; and (3) sufficient laser pump power in order to generate significant levels of available DFG power.

- *Dye and Ti:Sapphire lasers*: Commercially available CW dye and Ti:Sapphire (Ti:Al_2O_3) laser, optically pumped by an Ar^+ or frequency doubled diode pumped solid state laser, are widely tunable from the visible to the near infrared (580–1100 nm). They are usually employed as suitable DFG pump sources for use in laboratory based high-resolution infrared spectroscopy.
- *Diode lasers*: Numerous types of diode lasers are attractive for application in DFG-based gas sensor instrumentation. The wavelength tunability of DFB- or DBR-based diode lasers, however, are typically limited to a few nanometers. Improvement in wavelength tuning can be accomplished by using external-cavity structures. The output power of single mode diode lasers is usually limited and often not sufficient for use as a DFG pumping source. A high-power tunable single mode diode laser source can be obtained based on a master oscillator power amplification (MOPA) architecture using a semiconductor optical amplifier or fiber amplifier.
- *Fiber lasers*: Recently commercially available CW single mode fiber laser for the region of 1050 (Ytterbium doped) and 1550 nm (Erbium doped) offer the optimum choice to boost available pumping powers to achieve compact CW DFG source [90,91].

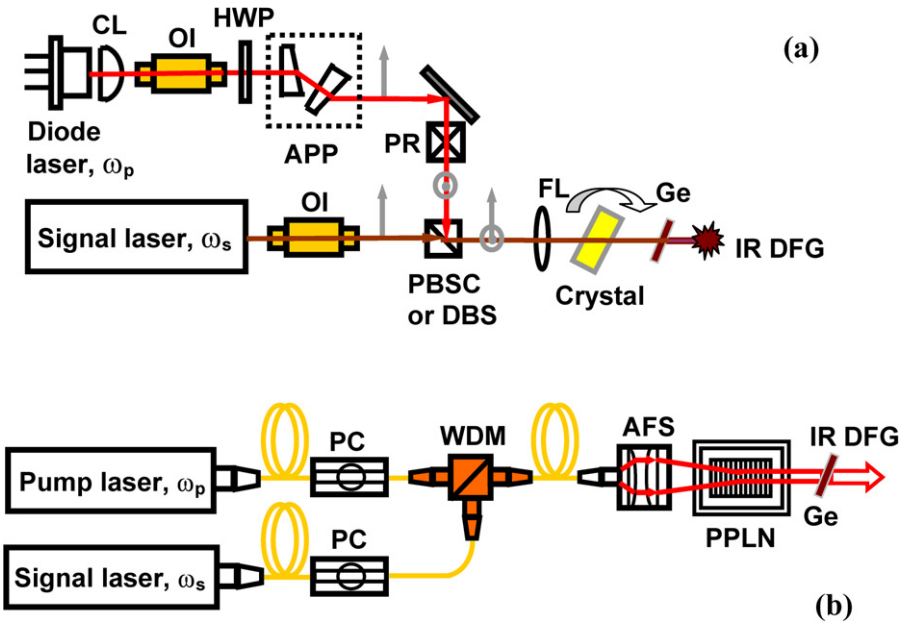

Fig. 7. Schematic of experimental set-up of DFG based on: (a) free space coupled laser beams, (b) fiber coupled laser beams. CL, collimating lens; OI, optical isolator; APP, anamorphic prism pair; FL, focusing lens; PR, polarization rotator; PBSC, polarizing beam splitter cube; DBS, dichroic beam splitter; Ge, germanium filter; PC, polarization controller; WDM, wavelength-division multiplexer; AFS, achromatic focusing system; HWP, half wave plate. PPLN, periodically poled $LiNbO_3$ in temperature-controlled oven.

3.4. Typical DFG architecture

Typical schematic diagrams of DFG architectures are shown in Fig. 7. The pumping sources consist usually of two lasers: one is a visible or near-IR laser (at ω_p as pump) and the other is a near-IR laser (at ω_s as signal). At least one of the two pump lasers should be tunable in wavelength for production of a tunable DFG source.

Fig. 7(a) shows an optical arrangement of DFG based on free space coupled laser beams [92,52,93]. Usually an optical isolator is used to prevent the laser from back-reflections. When a diode laser is used as pumping source, the following optical components are necessary for beam shaping: an anamorphic prism pair and a $\lambda/2$ plate to make laser beam profile circular and its polarization linear. It is worth noting that the laser beam transverse mode plays an important role in efficient coupling of the interacting waves. As pointed out in Ref. [94], the TEM_{11} beam mode coupling degrades the nonlinear optical frequency-conversion efficiency by more than a factor of 2 with respect to TEM_{00} mode coupling. For BPM, a polarization rotator is used in order to match the beam polarization to the crystal axis to fulfill the phase-matching condition. The orthogonal polarizations can then be combined by a polarizing beam splitter cube. In the case of an e–e=e QPM DFG process where all interacting waves are vertically, i.e. extraordinarily, polarized, polarization rotator is not useful and the laser beams can be combined by use of a dichroic beam splitter. Optimum optical alignment for overlapping the pumping beams is achieved by using a pin-hole technique and by checked with a beam analyzer camera.

When fiber-coupled lasers or fiber lasers are used as pump sources, a wavelength division multiplexer (WDM) [46,95,96] is employed for combining the laser beams as shown in Fig. 7(b). Optical fiber technology ensures optical alignment-free combining and spatial overlapping of laser beams, which translates into improved DFG power conversion by a factor of 2 [46].

Two laser beams are usually collinearly focused into a nonlinear optical crystal with a lens of focal length in the range of 50–350 mm (as a compromise between high laser intensities, by use of a lens with short focal length, and large effective interaction area with a long focus). Implementation of an achromatic Gaussian beam coupling optical system [92,52,96] will reduce the longitudinal chromatic aberration effect on the location of the focused Gaussian beam waists inside the nonlinear optical crystal which can result in an increase in infrared DFG power by a factor of 3.

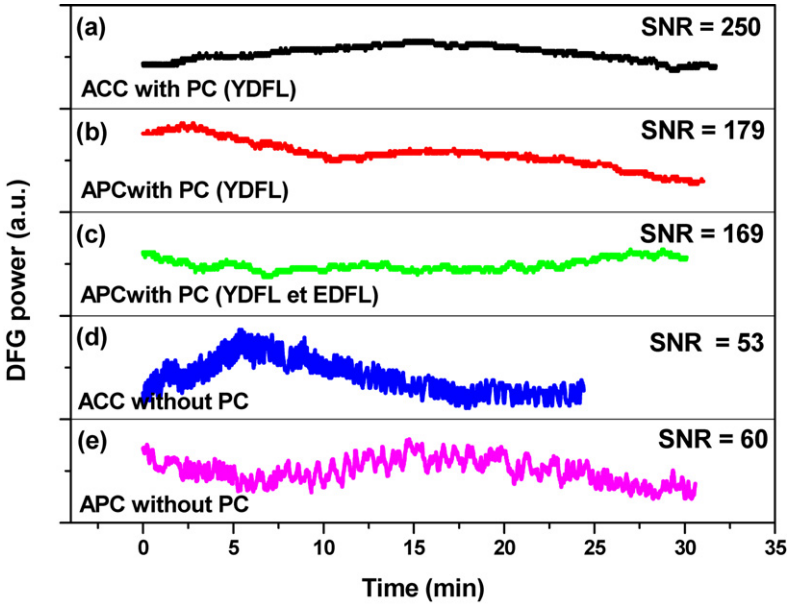

Fig. 8. Stabilization of DFG power with the help of polarization control (PC). ACC: laser in automatic current control (ACC) mode; APC: laser in automatic power control (APC) mode.

Instantaneous variation of the polarization state of the laser beams is an important instability source of the DFG power. Fig. 8 shows the effects of polarization of laser pumping beams on the stabilization of DFG output power with the help of polarization control (PC). The SNR of the DFG power gained approximately a factor of 5 with polarization control as compared to the case without polarization control (Fig. 8(a) vs. (d)) [96].

The crystal is operated at room temperature or adjustable elevated temperatures when temperature tuning is needed. In the case of using PPLN as frequency converter, it is worth noting that the crystal temperature should be $>100\,^{\circ}\mathrm{C}$ in order to avoid photorefractive damage.

A 1-mm thick germanium (Ge) filter is usually employed as a long-wavelength pass filter to block unwanted pump and signal laser beams. The filter can be set at the Brewster's angle to reduce the reflection losses of transmitted infrared beam.

The DFG light can be detected with a liquid-nitrogen-cooled or Peltier-cooled IR detector, such as InAs (1.0–3.8 μm), PbSe (2.0–6.0 μm), InSb (1.0–5.5 μm), HgCdTe PV (0.5–11.0 μm) or HgCdTe PC (1.0–26 μm). The output signal from the detector is amplified by means of a low-noise preamplifier.

Design consideration of DFG has been discussed in detail in Refs. [97,33,34].

3.5. Optical parametric radiation in the mid-IR (3–20 μm) by means of DFG

DFG has become a routine technique for optical parametric source generation for spectroscopic applications in the laboratory and in-situ field applications. Two spectral regions can be distinguished according to the specific nonlinear optical material used as frequency converter: the two 3–5 μm and 5–20 μm regions.

3.5.1. The 3–5 μm spectral region

The well established grating-engineered QPM PPLN technology in combination with a large damage threshold and high thermal conductivity, as well as the commercial availability make periodically poled ferroelectric materials suitable for efficient DFG in the 3–5 μm region [98–102,95,103,34,93,96,38]. Although periodically poled $LiNbO_3$ (PPLN) is the most used nonlinear optical material which makes QPM-DFG a practical technique for real world applications, periodically poled $RbTiOASO_4$ (PPRTA) offers several distinct advantages compared to PPLN: The optical transparency range for PPRTA extends to about 5.8 μm at long wavelengths, as compared to 5.5 μm for PPLN. PPRTA has the benefit of significantly reduced absorption in the 4–5 μm region, with a comparable nonlinear optical figure of merit (21.5 $\mathrm{pm}^2/\mathrm{V}^2$, for PPRTA vs. 27 $\mathrm{pm}^2/\mathrm{V}^2$ for PPLN). In addition, PPRTA possesses a high damage

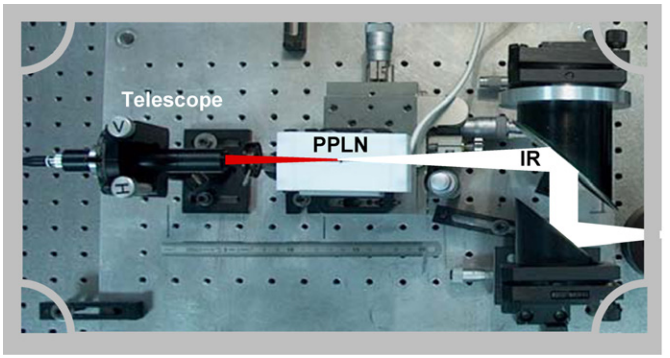

Fig. 9. A compact mid-IR laser source (2.96–3.60 μm) based on fiber laser pumped DFG in a PPLN crystal.

threshold of >400 MW/cm^2, which is five times higher than that for PPLN. Another advantage of PPRTA is that it possesses a lower coercive field for electric poling (∼ten times lower than that for PPLN), which facilitates periodic poling of several mm-thick samples with a significantly higher resistance to photorefractive damage than PPLN. This characteristic permits stable operation of PPRTA at room temperature. These characteristics are advantageous for nonlinear optical frequency-conversion when using high-power fiber amplifiers and diode-pumped solid-state lasers as DFG pumping sources [104–106].

The CW DFG output power based on periodically poled materials are in general in the range of 10–100 μW. Alternatively, average power levels above 1 mW have been reported for a DFG system that uses a combination of a pulsed pump and a CW signal source [107].

The use of well developed telecommunications diode lasers, fiber amplifiers, optical fiber delivery systems and fiber couplers has led to the realization of compact and robust laser instruments based on DFG in PPLN for trace gas detection application. CW DFG power scaling to the mW level has been recently achieved: 3.5-mW at 3.35 μm produced from a PPLN crystal pumped with high laser pump powers ($P_p = 550$ mW and $P_s = 3.9$ W) [90], and 15-mW DFG power at 3.52 μm generated in an efficient ridge waveguide PPLN crystal using $P_p = 320$ mW and $P_s = 520$ mW [70].

Fig. 9 shows a compact mid-IR laser source (2.96–3.60 μm) by DFG in a PPLN crystal [96].

3.5.2. The 5–20 μm region

Due to the lack of suitable QPM materials, DFG in this spectral region is usually realized by BPM using semiconductor materials including $AgGaS_2$ [31,32,47,108–111], $AgGaSe_2$ [112,113], GaSe [114,51,92] and $ZnGeP_2$ [115, 116]. Long-wave IR up to ∼19 μm has been achieved by DFG in GaSe crystal. Experiments of DFG based on biaxial crystals such as $LiInS_2$ [48] and $LiInSe_2$ [117] have been recently performed by type II BPM in the X–Y plane. Compared to $AgGaS_2$ that is largely used for DFG in the 5–11 μm region, $LiInS_2$ and $LiInS_2$ possess larger thermal conductivity (∼3–4 times larger) and larger energy gap (3.59 eV for $LiInS_2$ compared to 2.6 eV for $AgGaS_2$) in combination with high damage threshold and relatively high nonlinear optical susceptibility. Furthermore, as these crystals crystallize in an mm2 space group (such as KTP) and are related to pyroelectrics, they will be promising materials for deep IR QPM operation if polarization domain reversal can be realized.

During the last several years, QPM materials based on orientation patterned GaAs (OP-GaAs) have been developed for DFG in the 8–12 μm [118]. DFG power levels of ∼μW has been produced at 8.4 μm region by mixing two telecom lasers ($\lambda_p = 1300$ nm and $\lambda_s = 1550$ nm) in a 19-mm long and 0.5-mm thick OP-GaAs crystal. Another QPM scenario using total internal reflection in ZnSe has been explored at ONERA (France) for DFG (in a pulsed regime) in the 8–13 μm spectral region [119].

The DFG output powers scale from some tens of nW to several μW. These relatively low DFG powers, compared to that obtained by DFG in the 3–5 μm, are mainly due to the lack of high efficient QPM crystals and because the DFG powers are inversely proportional to the square of infrared wavelength λ_i.

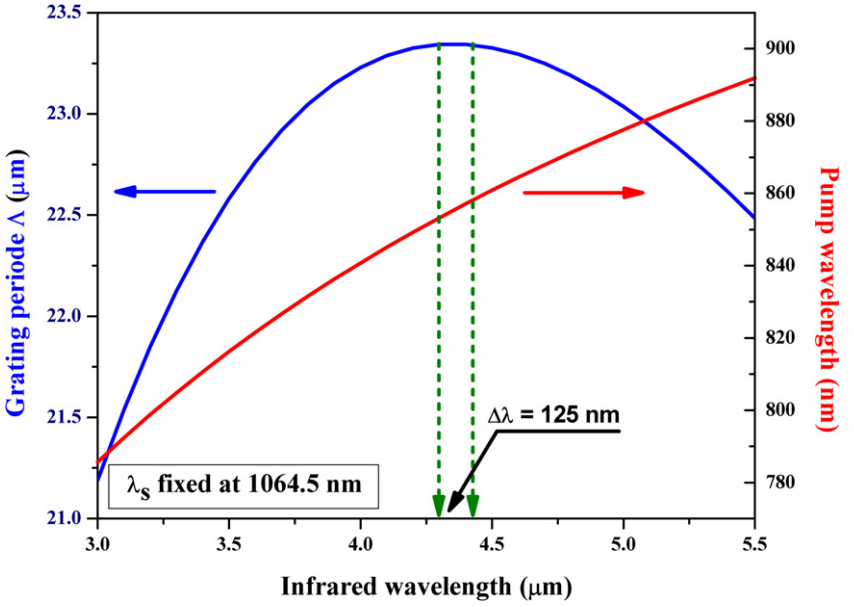

Fig. 10. QPM-DFG characteristics in a PPLN crystal at room temperature. Shown is the generated infrared wavelength as a function of the pump laser wavelength and the grating period Λ (with the signal laser fixed at 1064.5 nm). As shown in the figure, at the QPM degeneracy point, a phase-matched bandwidth of 125 nm could be obtained around 4.4 μm.

3.6. Characteristics of DFG-based optical parametric coherent light

3.6.1. Phase-matched DFG wavelength acceptance bandwidth

Wavelength tunability is one of the most important characteristic parameters of laser source for use in applied spectroscopy, in particular for trace gas sensing when spectroscopic detection of multispecies and broadband absorbers is required. DFG-based infrared wavelength tuning is usually achieved by scanning the wavelength of one laser while the other is held fixed. In this case, the infrared wavelength tuning is limited by phase mismatch effects (see Fig. 3). The phase-matching bandwidth BW (FWHM) is inversely proportional to the crystal length and can be written as [120]:

$$\mathrm{BW}(\mathrm{cm}^{-1}) = \left\{ L_{\mathrm{eff}} \left[(n_i - n_s) + \left(\lambda_s \frac{\partial n_s}{\partial \lambda_s} - \lambda_i \frac{\partial n_i}{\partial \lambda_i} \right) \right] \right\}^{-1} \tag{8}$$

where L_{eff} is the equivalent crystal length (in cm).

In order to improve the DFG spectral tunability, a method based on synchronous scanning of the two pumping laser wavelengths was developed which maintains the wavelength-dependent PM condition over a long infrared frequency scan. This was achieved by scanning two laser wavelengths with an appropriate slope ratio: '$\Delta\omega_s/\Delta\omega_i$-to-$\Delta\omega_p/\Delta\omega_i$' [47]. In a QPM scheme, wide acceptance bandwidth can be obtained for quasi-phase-matched DFG at the QPM degeneracy point where $\mathrm{d}\Lambda/\mathrm{d}\lambda = 0$ as shown in Fig. 10. In this case, the QPM bandwidths are more than two orders of magnitude larger than those observed in BPM-DFG. A bandwidth of 500 nm around 4.3 μm wavelength has been reported for QPM-DFG in PPLN near the degeneracy point [121].

Fig. 11 shows a QPM-DFG frequency scan as wide as 62 cm^{-1} (FWHM) near 4.2 μm, allowing record of an absorption spectrum of carbon dioxide of the whole ν_3 band with a single phase-matched frequency scan [122]. Temperature-dependent quasi-phase-matched DFG wavelength acceptance bandwidth, as shown in Fig. 12, has been recently studied and characterized [122].

3.6.2. Phase-matched acceptance angle for BPM with angle-tuning

Phase-matching sets a limit to the angle acceptance, $\Delta\theta_{\mathrm{BW}}$, which determines the maximum permissible divergence. The phase-matched acceptance angle can be estimated with [123]:

$$\Delta\theta_{\mathrm{BW}}(\mathrm{FWHM}) = \frac{5.568\lambda_i n_o^2(\lambda_i) n_e^2(\lambda_i)}{\pi L_{\mathrm{eff}} n_e^3(\lambda_i, \theta)[n_o^2(\lambda_i) - n_e^2(\lambda_i)] \sin 2\theta} \tag{9}$$

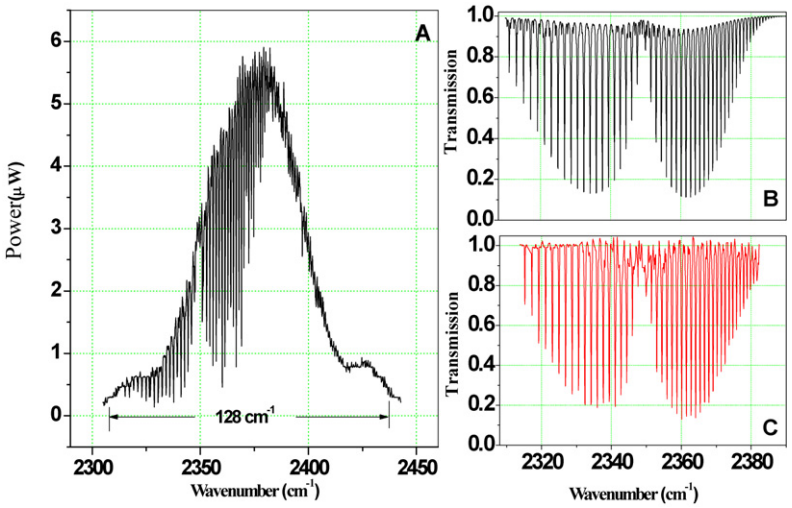

Fig. 11. Wide DFG scan of the CO_2 absorption spectrum: Panel (A), where the signal laser was fixed at 1064 nm and the pump laser wavelength was scanned from 844.8 nm to 854.9 nm. The grating period and temperature of the PPLN crystal were fixed at 22.5 μm and 181 °C, respectively. Panel (B) is the simulated absorption spectrum using the HITRAN 04 database and panel (C) is the measured spectrum after numerical signal processing.

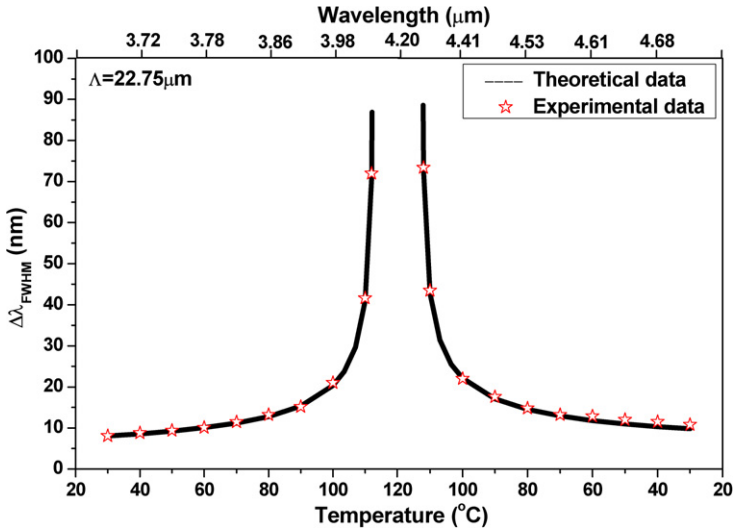

Fig. 12. Temperature-dependent DFG wavelength tuning bandwidth: Λ is fixed at 22.75 μm with temperature increasing from 30 to 110 °C with 10 °C increments.

The angular acceptance bandwidth varies inversely with effective crystal length L_{eff}. Fig. 13 depicts the phase-mismatching limited angle bandwidth $\delta\theta_{\text{BW}}$(FWHM). A value of $\delta\theta_{\text{BW}} = 0.39°$ was obtained for type II BPM DFG in $LiInS_2$ crystal in the X–Y plane at $\lambda_{\text{IR}} = 7$ μm.

3.6.3. Phase-matching calculation

Phase-matched pumping laser wavelengths, as well the phase-matched crystal angle, can be calculated using the Sellmeier equation (i.e. Eq. (5)). The Sellmeier parameters are generally determined by fitting the measured wavelength-dependent indices of refraction with a precision of $\Delta n \sim 10^{-4}$ using a minimum-deviation technique [124,125]. This precision, however, is usually not accurate enough for the prediction of phase-matched wavelengths in a CW parametric interaction. Differences in the laser frequencies between the predicted values and the experimental data are typically $\sim$100 cm^{-1}. Usually the wavelength-dependent dispersion equation should be further

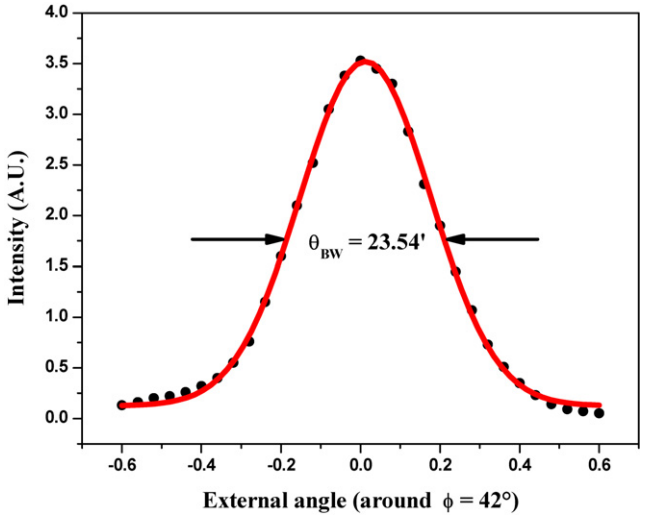

Fig. 13. Angular bandwidth for type II PM DFG in a $LiInS_2$ crystal in the X–Y plane. Filled circles, experimental data; solid curve, calculated data based on a plane-wave model. The angle acceptance bandwidth of ∼0.39° was observed at 7 μm.

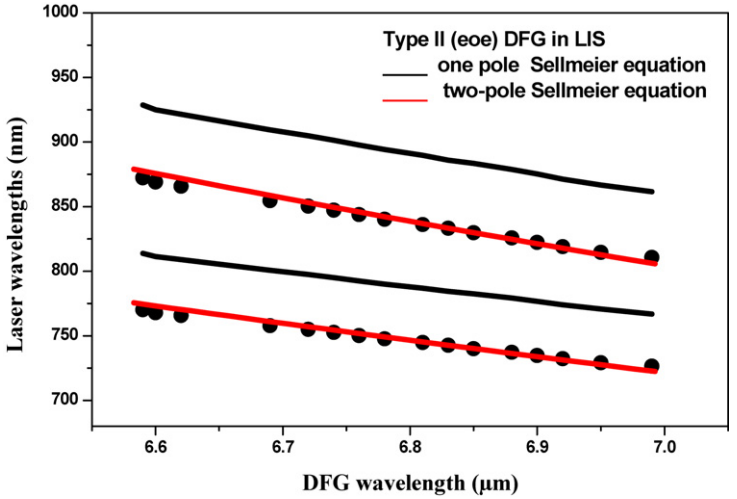

Fig. 14. Phase-matched pump and signal laser wavelengths for $LiInS_2$-based DFG in the 6.6–7.0 μm spectral region (φ fixed at 42°). Black and red (lighter line) curves represent calculated values based on a one-pole Sellmeier equation deduced from Ref. [126] and from the improved equation in [48], respectively. The filled circles indicate experimental data. (For interpretation of the references to color in this figure legend, the reader is referred to the web version of this article.)

improved by using experimentally measured PM wavelength data [52]. Fig. 14 depicts experimental phase-matched laser wavelengths (filled circles) for DFG from 6.6 to 7.0 μm (with $\varphi = 42°$) [48]. The predicted values based on a one-pole Sellmeier equation deduced from Boyd's refractive-index data [126] are plotted for comparison (black curves). As can be seen, the deviations from the calculated curves are considerable. As Fig. 14 implies, an appreciable offset of $\Delta\lambda = \lambda_{cal} - \lambda_{exp} = 45$ nm for the pump and the signal wavelengths was observed. Based on the experimental type II DFG data combined with the experimental type II second harmonic generation angles measured in the fundamental wavelength ranging from 2.5 to 6 μm, the Sellmeier equation has been improved by using a two-pole dispersion equation [127]. Excellent agreement between the experimental data and the theoretical prediction was obtained, as shown by the red (lighter) curves in Fig. 14.

The temperature effects on phase-matching characteristics are important to consider, since they will shift the PM condition, i.e. the phase-matched pumping frequency. For instance: shifting of $-0.7\ cm^{-1}/°C$ for $AgGaS_2$ [47],

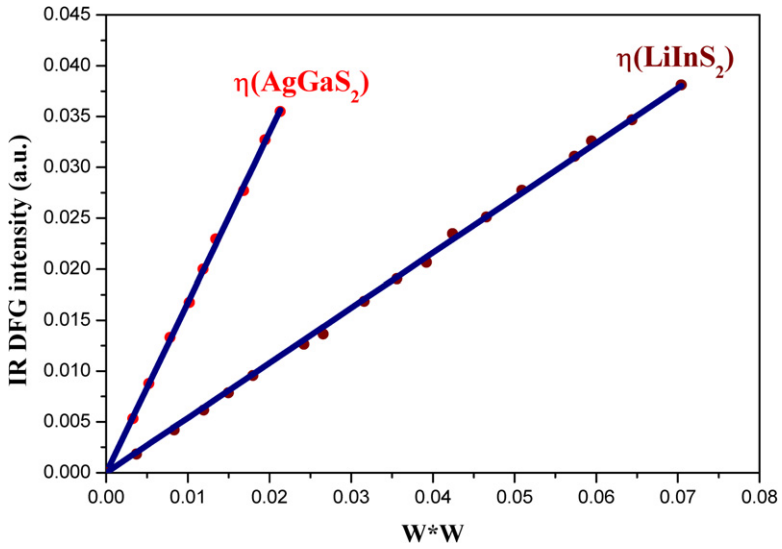

Fig. 15. Measurements of DFG power conversion efficiencies for $AgGaS_2$ and $LiInS_2$: dots, experimental data; curve, linear fit.

$-1.02\ \mathrm{cm}^{-1}/^{\circ}\mathrm{C}$ [105] and $-0.05\ \mathrm{cm}^{-1}/^{\circ}\mathrm{C}$ for $LiInS_2$ [48] have been measured. Pumping power-induced thermal effects are the dominant factor that change crystal temperature and thus results in DFG output power fluctuations.

3.6.4. DFG power conversion efficiency

The power conversion efficiency of DFG, defined as $\eta = P_{\mathrm{IR}}/(P_p \times P_s)$, can be experimentally derived from a linear fit of the plot of the generated DFG intensity versus the product of two pumping laser powers. In general, the DFG power conversion is ∼several hundreds of $\mu\mathrm{W}/\mathrm{W}^2$ for the 3–5 μm region using QPM ferroelectric materials and ∼several $\mu\mathrm{W}/\mathrm{W}^2$ for the 5–10 μm region using semiconductor crystals.

In the work reported in Ref. [48], the absolute value of d_{eff} of the $LiInS_2$ (LIS) crystal was determined relative to the known value d_{36} of $AgGaS_2$ (AGS) based on measurements of the power conversion efficiencies, shown in Fig. 15. The DFG power conversion efficiency η was calculated by taking into account all optical losses for LIS- and AGS-based DFG, respectively, under identical experimental conditions. Then the ratio between the nonlinear coefficient of LIS and that of AGS can be derived on the basis of Eq. (1):

$$\frac{d^2_{\mathrm{eff}}(\mathrm{AGS})}{d^2_{\mathrm{eff}}(\mathrm{LIS})} = \frac{\eta_{\mathrm{AGS}}}{\eta_{\mathrm{LIS}}} \times \frac{(n_i n_s n_p)_{\mathrm{AGS}}}{(n_i n_s n_p)_{\mathrm{LIS}}} \times \frac{\omega_i^2(\mathrm{LIS})}{\omega_i^2(\mathrm{AGS})} \times \frac{(\lambda_s/n_s + \lambda_p/n_p)_{\mathrm{AGS}}}{(\lambda_s/n_s + \lambda_p/n_p)_{\mathrm{LIS}}} \times \frac{\mathrm{e}^{\alpha L}(\mathrm{AGS})}{\mathrm{e}^{\alpha L}(\mathrm{LIS})} \times \frac{h_{\mathrm{LIS}}}{h_{\mathrm{AGS}}} \tag{10}$$

We obtained a $d_{\mathrm{eff}} = 6.9 \pm 0.8\ \mathrm{pm/V}$ for LIS at ∼7 μm at room temperature. This value is in good agreement with the values of $d_{\mathrm{eff}} = 6.54\ \mathrm{pm/V}$, deduced from a femtosecond second harmonic generation process [128].

4. Mid-IR difference-frequency generation based source for spectroscopic applications

The performance characteristics of DFG-based optical parametric sources have greatly advanced during the past decade. This new type source has become an attractive and useful mid-IR laser source for ultra-sensitive spectroscopic applications. These include such diverse fields as:

(1) Environmental and industrial applications: detection of atmospheric H_2CO [129,130], CH_4 [131] and N_2O [132]; measurements of volcanic gases [133], vapor-phase benzene [134,96] and toluene [135]; in situ and on-line monitoring of CO in an industrial glass furnace [136], measurements of CO in the exhaust stream of a reactor [137], tomographic imaging of CO in laminar flames [138] and time-resolved hydrocarbon fuel measurements [139];
(2) Atmospheric chemistry: airborne measurements of H_2CO [95];
(3) Molecular spectroscopy: study of molecular lineshapes and line parameters [140–145], polarization spectroscopy for CH_4 detection [146], sub-Doppler molecular spectroscopy [90] and spectroscopy of the $\nu_1 + \nu_3$ band of N_2O [140];

(4) Breath analysis for biomedical applications [147,148];
(5) Isotopic ratio measurements of $^{13}CO_2/^{12}CO_2$ [149], $^{13}CH_4/^{12}CH_4$ [106,150] and $^{15}N^{14}N^{16}O/^{14}N_2{}^{16}O$ [151].

The wide spectral tunability permits multicomponent detection of atmospheric trace gases and toxic organic chemical species, and allows convenient access to infrared probing wavelengths suitable for sensitive and selective trace gas detection, which is important for the detection and quantification of volatile organic compounds whose spectral absorption lines are usually unresolved and cover a large spectral range of tens of cm^{-1}. The availability of relatively high DFG power scaling from some tens of μW to the mW level enables DFG-based laser instruments to achieve high sensitivity in conjunction with ultra-sensitive spectroscopic detection techniques based on [152,37]:

(1) long optical pathlength spectroscopy: Herriott or White multipass cell [153,95,154,34,106,155,132,96,156], cavity ring-down and cavity enhanced spectroscopy [103,157,118,158];
(2) a low noise approach, such as wavelength modulation spectroscopy [131,151] or two-tone frequency modulation spectroscopy [159];
(3) sensitive detection approach, like dual-beam balanced detection [51,160].

5. Summary and outlook

In this article we have summarized the current status of continuous-wave mid-infrared sources based on difference-frequency generation. Relevant issues encountered in phase-matching schemes, suitable laser pumping sources, DFG architecture, phase-matched frequency scanning, extension of phase-matchable infrared spectral coverage and power conversion efficiency were discussed. DFG has proven to be a useful technique for coherent source generation in the infrared, which allows for the transfer of high performance of near infrared lasers to the mid-IR wavelength region. New trends in development of DFG technology can be summarized as follows:

5.1. High DFG power

High output power is highly desirable for DFG-based optical parametric laser sources, which permits overcoming inherent electronic detection noise and implement spectroscopic techniques, such as CRDS or photoacoustic spectroscopy (PAS) for ultra-sensitive detection. DFG power levels can be increased by means of the following methods:

(1) *High pumping power*: QPM-PPLN-based DFG provides an output power in the range of 10–100 μW by using modest pumping power levels of several hundreds of mW for both input lasers. Maddaloni et al. reported [90] high tunable mid-IR power scaling to 3.5 mW from DFG in a bulk PPLN crystal, pumped with 3.9 W and 550 mW for the signal and the pump lasers, respectively.
(2) *High frequency conversion efficiency*: Waveguide QPM-PPLN offers a higher conversion efficiency than bulk QPM-PPLN [73]. Recently, highly efficient 3-μm DFG has been realized using a direct-bonded QPM $LiNbO_3$ ridge waveguide. DFG power levels as high as 15 mW were obtained at 3.52 μm, with an external conversion efficiency of up to 19% W^{-1} [70].
(3) *DFG in quantum well material*: Alternatively, intersubband quantum wells materials are important promising materials for a high conversion efficiency nonlinear optical process, the second order nonlinear susceptibility $\chi^{(2)}$ is several order of magnitude larger than for bulk media. Chui et al. [161] have demonstrated DFG in intersubband InGaAs/AlAs quantum wells for the 8–12 μm region. DFG $\chi^{(2)}$ of 12 nm/V at 9.5 μm was observed, more than 65 times that of bulk GaAs (180 pm/V).
(4) *Monolithic DFG*: Chou et al. reported a new waveguide scheme with an integrated coupling structure for wavelength conversion within the 1.5-μm band based on DFG in $LiNbO_3$ waveguide: the pump and the signal are coupled into the wavelength conversion region via a mode filter-adiabatic taper and a directional coupler, implemented with periodically segmented waveguides [72].
(5) *Pigtailed PPLN*: DFG power could be further increased via the improvement in the coupling efficiency of the input laser power to the crystal, by means of the use of a pigtailed waveguide PPLN device that is commercially available.

5.2. Broad bandwidth of phase-matched DFG

Wide phase-matched DFG bandwidths are important for spectroscopic applications such as high-resolution molecular spectroscopy or trace gas detection of multispecies and broadband absorbers. PM bandwidth is usually limited by phase-mismatching effects, as discussed above. Recently, by the use of apodization in a QPM $LiNbO_3$ ridge waveguide, phase-matched DFG wavelength tuning as large as 60 nm (FWHM) in the 3.4 μm band has been achieved with a flat PM response and a DFG conversion efficiency of 2% W^{-1} [162].

5.3. Efficient DFG in the deep mid-IR

High frequency down-conversion efficiencies can be obtained through the use of QPM devices. DFG-based infrared light at long wavelength is subject to an important limitation by its relatively low generation power (0.01–1 μW) using a BPM scheme in semiconductor materials, due to the lack of suitable QPM media. QPM devices based on orientation-patterned GaAs have been developed at Stanford University. High efficient DFG in the 7–9 μm region has been achieved through the use of the QPM OP-GaAs crystal. DFG powers of several μW have been produced [118]. Developments are in progress [174,175], which include realization of multi-period OP-GaAs crystal for wide spectral coverage and use of AR coatings to minimize optical losses from the crystal facets.

Recently, a relaxor-based ferroelectric single crystal of $Pb(Mg_{1/3}Nb_{2/3})_{0.62}Ti_{0.38}O_3$ (PMNT) has been investigated [163,164]. PMNT crystal offers several attractive optical properties: it is optically transparent from 0.4 to 9 μm and the coercive field for PMNT is about 2–3 kV/mm (compared to 21 kV/mm for $LiNbO_3$). Characterization of optical and nonlinear optical properties of PMNT in order to determine its application in nonlinear optical devices is in progress.

5.4. Monolithic DFG with pump lasers

In order to alleviate complexity in a traditional discrete DFG design, recent efforts were carried out on the integration of DFG process into a laser semiconductor:

(1) *self-DFG in Cr:ZnSe* [165]: self-difference frequency mixing in a gain switched Cr:ZnSe laser using Fresnel phase matching (FPM) has been investigated in pulsed regime. Taking advantage of both the lasing and the nonlinear properties of Cr:ZnSe, the authors used a single pump beam at 1.9 μm to pump the Cr^{2+} laser transition $^5E \rightarrow {}^5T_2$, yielding laser emission at 2.4 μm. Difference frequency mixing occurs between the pump beam and the laser beam to produce mid-IR radiation in the 9 μm range using a FPM scheme in ZnSe.
(2) *DFG in quantum cascade laser* [166]: DFG from two-wavelength, two-stack QCLs with integrated nonlinearities was recently reported. Radiation at the difference frequency ($\lambda = 13.3$ μm) was detected from a two-wavelength ($\lambda = 5.3$ μm and 8.8 μm) QCL processed with a split ridge configuration.

After almost a decade of development, DFG-based mid-infrared laser is now commercially available from NovaWave (IRIS™ 1000, [167]). The IRIS™ 1000 laser produces single frequency (MHz linewidth) and transverse mode (TEM_{00}), stable infrared laser light without the use of cryogens and provides mode-hop free tuning in the "fingerprint" C–H, N–H, and O–H stretch region of the mid-IR (3.2–3.6 μm) with an output power ranging from 150 μW to mW. It is suitable for spectroscopic applications such as Doppler limited high resolution spectroscopy and trace gas monitoring. The system features on-board touch screen computer control with Ethernet remote control capability. More recently, 65-mW 3.4 μm tunable DFG has been achieved using damage resistant Zn:$LiNbO_3$ waveguide, reported by Asobe et al. [168] at CLEO-Europe 2007, ∼5 months after the previous record of 15-mW DFG power was published [70]. The high CW single-frequency output power combined with additional merits transferred directly from high performance characteristics of the pump lasers (large frequency tunability, narrow linewidth, wide spectral coverage and room temperature operation) will make DFG-based laser sources an attractive alternative choice to lead-salts diode lasers, quantum cascade lasers and optical parametric oscillators in the mid-infrared spectral region from 3 to 5 μm and beyond.

As tunable laser pump sources and QPM materials evolve, difference-frequency generation technology will continue to advance and impact the development of optical parametric laser sources for various real world applications.

Acknowledgements

This work is supported in part by the European program INTERREG (EDER French grants n° 111/118), the FNS program ACI (CNRS-DGA/NMAC/10) and the BQR program of the Université du Littoral Côte d'Opale. M. Gao acknowledges the financial support from the French International Programme of Scientific Cooperation (CNRS/PICS n° 3359).

References

[1] G. Phillips, P. Hinske, W. Demtröder, K. Möllmann, R. Beigang, Appl. Phys. B 47 (1988) 127–133.
[2] Ch. Hornberger, M. König, S.B. Rai, W. Demtröder, J. Chem. Phys. 190 (1995) 171–177.
[3] S.-C. Hsu, R.H. Schwendeman, G. Magerl, IEEE J. Quantum Electron. QE-24 (1988) 2294–2301.
[4] G. Magerl, W. Schupita, E. Bonek, IEEE J. Quantum Electron. QE-18 (1982) 1214–1220.
[5] A. Romann, M.W. Sigrist, Appl. Phys. B 75 (2002) 377–383.
[6] P. Werle, Spectrochimica Acta A 54 (1998) 197–236.
[7] P.J. McCann, Y. Selivanov, Mater. Res. Soc. Symp. Proc. 891 (2006), 0891-EE01-05.
[8] L. Coldren, IEEE J. Select. Topics Quantum Electron. 6 (2000) 988–999.
[9] http://www.ekipstech.com.
[10] J. Faist, F. Capasso, D.L. Sivco, C. Sirtori, A.L. Hutchinson, A.Y. Cho, Science 264 (1994) 553–555.
[11] F. Capasso, C. Gmachl, A. Tredicucci, A.L. Hutchinson, D.L. Sivco, A.Y. Cho, OPN 10 (1999) 32–37.
[12] J.S. Yu, S. Slivken, S.R. Darvish, A. Evans, B. Gokden, M. Razeghi, Appl. Phys. Lett. 87 (2005) 041104.
[13] A. Evans, J. Nguyen, S. Slivken, J.S. Yu, S.R. Darvish, M. Razeghi, Appl. Phys. Lett. 88 (2006) 051105.
[14] http://www.alpeslasers.ch.
[15] G. Wysocki, R.F. Curl, F.K. Tittel, F. Capasso, L. Diehl, M. Troccoli, G. Höfler, R. Maulini, J. Faist, in: Conference on Lasers and Electro-Optics/Quantum Electronics and Laser Science Conference and Photonic Applications Systems Technologies 2007 Technical Digest, Optical Society of America, Washington, DC, 2007, CFB3.
[16] R.Q. Yang, Superlattices Microstruct. 17 (1995) 77–83.
[17] J.H. Miller, Y.A. Bakhirkin, T. Ajtai, F.K. Tittel, C.J. Hill, R.Q. Yang, Appl. Phys. B 85 (2006) 391–396.
[18] L.E. Christensen, C.R. Webster, R.Q. Yang, Appl. Opt. 46 (2007) 1132–1138.
[19] R.Q. Yang, J.L. Bradshaw, J.D. Bruno, J.T. Pham, D.E. Wortman, R.L. Tober, Appl. Phys. Lett. 81 (2002) 397–399.
[20] R.Q. Yang, C.J. Hill, B.H. Yang, C.M. Wong, R.E. Muller, P.M. Echternach, Appl. Phys. Lett. 84 (2004) 3699–3701.
[21] R.Q. Yang, C.J. Hill, B.H. Yang, Appl. Phys. Lett. 87 (2005) 151109.
[22] K. Mansour, Y. Qiu, C.J. Hill, A. Soibel, R.Q. Yang, Electron. Lett. 42 (2006) 1034–1035.
[23] M.H. Dunn, M. Ebrahimzadeh, Science 286 (1999) 1513–1517.
[24] G.A. Turnbull, D. McGloin, I.D. Lindsay, M. Ebrahimzadeh, M.H. Dunn, Opt. Lett. 25 (2000) 341–343.
[25] M. Ebrahimzadeh, in: I.T. Sorokina, K.L. Vodopyanov (Eds.), Topics in Appl. Phys., vol. 89, Springer-Verlag, Berlin–Heidelberg–New York, 2003, pp. 179–213.
[26] M.M.J.W. Herpen, S. Li, S.E. Bisson, F.J.M. Harren, Appl. Phys. Lett. 81 (2002) 1157–1159.
[27] M.M.J.W. Herpen, S.E. Bisson, A.K.Y. Ngai, F.J.M. Harren, Appl. Phys. B 78 (2004) 281–286.
[28] A.K.Y. Ngai, S.T. Persijn, G. von Basum, F.J.M. Harren, Appl. Phys. B 85 (2006) 173–180.
[29] A. Henderson, R. Stafford, Opt. Express 14 (2006) 767–772.
[30] A.S. Pine, J. Opt. Soc. Am. 64 (1974) 1683–1690.
[31] P. Canarelli, Z. Benko, R.F. Curl, F.K. Tittel, J. Opt. Soc. Am. B 9 (1992) 197–202.
[32] A.H. Hielscher, C.E. Miller, D.C. Bayard, K.P. Smolka, R.F. Curl, F.K. Tittel, J. Opt. Soc. Am. B 9 (1992) 1962–1967.
[33] D. Richter, P. Weibring, Appl. Phys. B 82 (2006) 479–486.
[34] P. Weibring, D. Richter, A. Fried, J.G. Walega, C. Dyroff, Appl. Phys. B 85 (2006) 207–218.
[35] W. Chen, D. Boucher, F. Tittel, Recent advances in continuous-wave laser difference-frequency generation in the mid-infrared: State of the art, applications, and perspectives, in: Recent Research Developments in Applied Physics, vol. 2, Transworld Research Network, 2002, pp. 27–68.
[36] C. Fischer, M.W. Sigrist, in: I.T. Sorokina, K.L. Vodopyanov (Eds.), Topics in Appl. Phys., vol. 89, Springer-Verlag, Berlin–Heidelberg–New York, 2003, pp. 97–140.
[37] F.K. Tittel, D. Richter, A. Fried, in: I.T. Sorokina, K.L. Vodopyanov (Eds.), Topics in Appl. Phys., vol. 89, Springer-Verlag, Berlin–Heidelberg–New York, 2003, pp. 445–510.
[38] H. Waechter, M.W. Sigrist, in: F. Träger (Ed.), Springer Handbook of Lasers and Photonics, Springer, Berlin, Heidelberg, 2007, pp. 801–814.
[39] J.A. Armstrong, N. Bloembergen, J. Ducuing, P.S. Pershan, Phys. Rev. 127 (1962) 1918–1939.
[40] G.D. Boyd, D.A. Kleinman, J. Appl. Phys. 39 (1968) 3597–3642.
[41] T. Chu, M. Broyer, J. Phys. 4 (1985) 523–533.
[42] J.-J. Zondy, Opt. Commun. 149 (1998) 181–206.
[43] E.J. Canto-Said, M.P. McCann, P.G. Wigley, G.J. Dixon, Opt. Lett. 20 (1995) 1268–1270.
[44] U. Simon, S. Waltman, I. Loa, F.K. Tittel, L. Goldberg, J. Opt. Soc. Am. 12 (1995) 323–327.
[45] K. Petrov, S. Waltman, R. Curl, F. Tittel, L. Hollberg, Appl. Phys. B 61 (1995) 553–558.

[46] D. Richter, Ph.D. dissertation, Rice University, 2000.
[47] W. Chen, J. Burie, D. Boucher, Rev. Sci. Instrum. 67 (1996) 3411–3415.
[48] W. Chen, E. Poullet, J. Burie, D. Boucher, M.W. Sigrist, J.-J. Zondy, L. Isaenko, A. Yèlisseyev, S. Lobanov, Appl. Opt. 44 (2005) 4123–4129.
[49] http://www.eksma.lt.
[50] V.G. Dmitriev, G.G. Gurzadyan, D.N. Nikogosyan, Handbook of Nonlinear Optical Crystals, Springer Series in Optical Science, vol. 64, Springer, Berlin/New York, 1997.
[51] W. Chen, G. Mouret, D. Boucher, Appl. Phys. B 67 (1998) 375–378.
[52] W. Chen, J. Burie, D. Boucher, Spectrochimica Acta A 55 (1999) 2057–2075.
[53] W.K. Burns, W. McElhanon, L. Goldberg, IEEE Photon. Technol. Lett. 6 (1994) 252–254.
[54] L.E. Myers, R.C. Eckardt, M.M. Fejer, R.L. Byer, W.R. Bosenberg, J.W. Pierce, J. Opt. Soc. Am. B 12 (1995) 2102–2116.
[55] L.E. Myers, Periodically poled materials for nonlinear optics, in: D.M. Finlayson, B.D. Sinclair (Eds.), Advances in Lasers and Applications, SUSSP Publications, 1999, pp. 141–180.
[56] L.E. Myers, M.L. Bortz, M.A. Arbore, R.C. Eckardt, M.M. Fejer, R.L. Byer, OPN 6 (1995) 30–31.
[57] L.E. Myers, R.C. Eckardt, M.M. Fejer, R.L. Byer, Opt. Lett. 21 (1996) 591–593.
[58] P.E. Powers, T.J. Kulp, S.E. Bisson, Opt. Lett. 23 (1998) 159–161.
[59] J.R. Kurz, X.P. Xia, M.M. Fejer, Opt. Lett. 27 (2002) 1445–1447.
[60] L.A. Eyres, P.J. Tourreau, T.J. Pinguet, C.B. Ebert, J.S. Harris, M.M. Fejer, B. Gerard, E. Lallier, Stanford University Annual Report, 1998–1999 (1999) 37.
[61] L.A. Eyres, P.J. Tourreau, T.J. Pinguet, C.B. Ebert, J.S. Harris, M.M. Fejer, L. Becouarn, B. Gerard, E. Lallier, Appl. Phys. Lett. 79 (2001) 904–906.
[62] K.L. Vodopyanov, O. Levi, P.S. Kuo, T.J. Pinguet, J.S. Harris, M.M. Fejer, B. Gerard, L. Becouarn, E. Lallier, Opt. Lett. 29 (2004) 1912–1914.
[63] Z.L. Liau, D.E. Mull, Appl. Phys. Lett. 56 (1990) 737–739.
[64] L. Gordon, G.L. Woods, R.C. Eckardt, R.R. Route, R.S. Feigelson, M.M. Fejer, R.L. Byer, Electron. Lett. 29 (1993) 1942–1944.
[65] M.J. Angell, R.M. Emerson, J.L. Hoyt, J.F. Gibbons, L.A. Eyres, M.L. Bortz, M.M. Fejer, Appl. Phys. Lett. 64 (1994) 3107–3109.
[66] D. Zheng, L.A. Gordon, Y.S. Wu, R.K. Route, M.M. Fejer, R.L. Byer, R.S. Feigelson, Electrochem. Soc. 144 (1997) 1439–1441.
[67] D. Zheng, L.A. Gordon, Y.S. Wu, R.S. Feigelson, M.M. Fejer, R.L. Byer, K.L. Vodopyanov, Opt. Lett. 23 (1998) 1010–1012.
[68] E. Lallier, M. Brevignon, J. Lehoux, Opt. Lett. 23 (1998) 1511–1513.
[69] A. Mustellier, E. Rosencher, A. Godard, M. Baudrier, M. Lefebvre, G. Mennerat, Ph. Kupecek, Ph. Lemasson, Appl. Phys. Lett. 84 (2004) 4424–4426.
[70] D. Richter, P. Weibring, A. Fried, Opt. Express 15 (2007) 564–571.
[71] E.J. Lim, H.M. Hertz, M.L. Bortz, M.M. Fejer, Appl. Phys. Lett. 59 (1991) 2207–2209.
[72] M.H. Chou, J. Hauden, M.A. Arbore, M.M. Fejer, Opt. Lett. 23 (1998) 1004–1006.
[73] D. Hofmann, G. Schreiber, C. Haase, H. Herrmann, W. Grundkotter, R. Ricken, W. Sohler, Opt. Lett. 24 (1999) 896–898.
[74] O. Tadanaga, T. Yanagawa, Y. Nishida, H. Miyazawa, K. Magari, M. Asobe, H. Suzuki, Appl. Phys. Lett. 88 (2006) 061101.
[75] W. Denzer, G. Hancock, A. Hutchinson, M. Munday, R. Peverall, G.A.D. Ritchie, Appl. Phys. B 86 (2007) 437–441.
[76] S.J.B. Yoo, R. Bhat, C. Caneau, M.A. Koza, Appl. Phys. Lett. 66 (1995) 3410–3412.
[77] S.J.B. Yoo, C. Caneau, R. Bhat, M.A. Koza, A. Rajhel, N. Antoniades, Appl. Phys. Lett. 68 (1996) 2609–2611.
[78] A. Fiore, V. Berger, E. Rosencher, P. Bravetti, N. Laurent, J. Nagle, Appl. Phys. Lett. 71 (1997) 3622–3624.
[79] A. Fiore, V. Berger, E. Rosencher, P. Bravetti, J. Nagle, Nature 391 (1998) 463–466.
[80] P. Bravetti, A. Fiore, V. Berger, E. Rosencher, J. Nagle, O. Gauthier-Lafaye, Opt. Lett. 23 (1998) 331–333.
[81] H. Komine, W.H. Long, J.W. Tully, E.A. Stappaerts, Opt. Lett. 23 (1998) 661–663.
[82] R. Haïdar, Ph. Kupecek, E. Rosencher, Appl. Phys. Lett. 83 (2003) 1506–1508.
[83] R. Haïdar, N. Forget, P. Kupecek, E. Rosencher, J. Opt. Soc. Am. B 21 (2004) 1522–1534.
[84] M. Baudrier-Raybaut, R. Haïdar, Ph. Kepecek, Ph. Lemasson, E. Rosencher, Nature 432 (2004) 374–376.
[85] M. Baudrier-Raybaut, R. Haïdar, Ph. Kupecek, Ph. Lemasson, E. Rosencher, Nature 432 (2004) 374–376.
[86] E. Rosencher, C. R. Acad. Sci. (Paris) Série IV 1 (2000) 615–625.
[87] D.S. Hum, M.M. Fejer, C. R. Physique 8 (2007) 180–198.
[88] P.F. Bordui, M.M. Fejer, Annu. Rev. Mater. Sci. 23 (1993) 321–380.
[89] R.V. Ramaswamy, X. Cao, Nonlinear Opt. 4 (1993) 115.
[90] P. Maddaloni, G. Gagliardi, P. Malara, P. De Natale, Appl. Phys. B 80 (2005) 141–145.
[91] J. Cousin, P. Masselin, W. Chen, D. Boucher, S. Kassi, D. Romanini, P. Szriftgiser, Appl. Phys. B 83 (2006) 261–266.
[92] R.S. Putnam, D.G. Lancaster, Appl. Opt. 38 (1999) 1513–1522.
[93] L. Deng, X. Gao, Z. Cao, W. Chen, Y. Yuan, W. Zhang, Z. Gong, Opt. Commun. 268 (2006) 110–114.
[94] A. Ashkin, G.D. Boyd, J.M. Dziedzic, Phys. Rev. Lett. 11 (1963) 14–17.
[95] D. Richter, A. Fried, B.P. Wert, J.G. Walega, F.K. Tittel, Appl. Phys. B 75 (2002) 281–288.
[96] J. Cousin, W. Chen, D. Bigourd, D. Boucher, S. Kassi, D. Romanini, in preparation.
[97] U. Simon, Z. Benko, M.W. Sigrist, R.F. Curl, F.K. Tittel, Appl. Opt. 32 (1993) 6650–6654.
[98] K.P. Petrov, L. Goldberg, W.K. Burns, R.F. Curl, F.K. Tittel, Opt. Lett. 21 (1996) 86–88.
[99] D. Richter, D. Lancaster, R.F. Curl, W. Neu, F.K. Tittel, Appl. Phys. B 67 (1998) 347–350.
[100] M. Seiter, D. Keller, M.W. Sigrist, Appl. Phys. B 67 (1998) 351–356.
[101] K.P. Petrov, A.P. Roth, T.L. Patterson, T.P.S. Thoms, L. Huang, A.T. Ryan, D.J. Bamford, Appl. Phys. B 70 (2000) 777–782.

[102] D. Richter, D. Lancaster, F.K. Tittel, Appl. Opt. 39 (2000) 4444–4460.
[103] S. Stry, P. Hering, M. Mürtz, Appl. Phys. B 75 (2002) 297–303.
[104] K. Fradkin-Kashi, A. Arie, P. Urenski, G. Rosenman, Appl. Phys. B 71 (2000) 251–255.
[105] W. Chen, G. Mouret, D. Boucher, F. Tittel, Appl. Phys. B 72 (2001) 873.
[106] X. Gao, L. Deng, W. Chen, D. Boucher, F. Tittel, in: Conference on Lasers and Electro-Optics/Quantum Electronics and Laser Science Conference and Photonic Applications Systems Technologies 2006, Technical Digest, ISBN 1-55752-813-6, Optical Society of America, Washington, DC, 2006, JThC57.
[107] C. Fischer, M.W. Sigrist, Q. Yu, M. Seiter, Opt. Lett. 26 (2001) 1609–1611.
[108] H.-D. Kronfeldt, G. Basar, B. Sumpf, J. Opt. Soc. Am. B 13 (1996) 1859–1863.
[109] W. Schade, T. Blanke, U. Willer, C. Rempel, Appl. Phys. B 63 (1996) 99–102.
[110] D. Lee, T. Kaing, J.-J. Zondy, Appl. Phys. B 67 (1998) 363–367.
[111] A. Khorsandi, U. Willer, P. Geiser, W. Schade, Appl. Phys. B 77 (2003) 509–513.
[112] K. Petrov, R. Curl, F. Tittel, L. Goldberg, Opt. Lett. 21 (1996) 1451–1453.
[113] B. Sumpf, D. Rehle, T. Kelz, H.-D. Kronfeldt, Appl. Phys. B 67 (1998) 369–373.
[114] W.C. Eckhoff, R.S. Putnam, S. Wang, R.F. Curl, F.K. Tittel, Appl. Phys. B 63 (1996) 437–441.
[115] S. Haidar, K. Miyamoto, H. Ito, Opt. Commun. 241 (2004) 173–178.
[116] J. Saikawa, M. Miyazaki, M. Fujii, H. Ishizuki, T. Taira, in: Advanced Solid-State Photonics, in: OSA Technical Digest Series (CD), Optical Society of America, 2007, paper MB8.
[117] W. Chen, M.W. Sigrist, J.-J. Zondy, S. Tinturier, F. Borel, R. Bocquet, J. Burie, D. Boucher, L. Isaenko, A. Yelisseyev, S. Lobanov, in: Conference on Lasers and Electro-Optics/International Quantum Electronics Conference and Photonic Applications Systems Technologies, Optical Society of America, 2004, Technical Digest (CD), paper CFI2.
[118] S.E. Bisson, T.J. Kulp, O. Levi, J.S. Harris, M.M. Fejer, Appl. Phys. B 85 (2006) 199–206.
[119] R. Haïdar, Ph. Kupecek, E. Rosencher, R. Triboulet, Appl. Phys. Lett. 82 (2003) 1167–1169.
[120] R.L. Byer, R.L. Hebst, Parametric oscillation and mixing, in: Y.-R. Shen (Ed.), Nonlinear Infrared Generation, Springer-Verlag, 1977.
[121] L. Goldberg, W.K. Burns, R.W. McElhanon, Appl. Phys. Lett. 67 (1995) 2910–2912.
[122] L. Deng, X. Gao, Z. Cao, W. Zhang, Z. Gong, W. Chen, Opt. Commun. (2007), submitted for publication.
[123] R.L. Sutherland, Handbook of Nonlinear Optics, Marcel Dekker, Inc., New York, 1996.
[124] W.L. Bond, J. Appl. Phys. 36 (1965) 1674–1677.
[125] D.F. Nelson, R.M. Mikulyak, J. Appl. Phys. 45 (1974) 3688–3689.
[126] G.D. Boyd, H.M. Kasper, J.H. McFee, J. Appl. Phys. 44 (1973) 2809–2812.
[127] S. Fossier, S. Salaüm, J. Mangin, O. Bidault, I. Thénot, J.-J. Zondy, W. Chen, F. Rotermund, V. Petrov, P. Petrov, J. Henningsen, A. Yelisseyev, L. Isaenko, S. Lobanov, O. Balachninaite, G. Slekys, V. Sirutkaitis, J. Opt. Soc. Am. B 21 (2004) 1981–2007.
[128] G. Knippels, A. van der Meer, A. Macleod, A. Yelisseyev, L. Isaenko, S. Lobanov, I. Thénot, J.-J. Zondy, Opt. Lett. 26 (2001) 617–619.
[129] D. Rehle, D. Leleux, M. Erdelyi, F.K. Tittel, M. Fraser, S. Friedfeld, Appl. Phys. B 75 (2001) 947–952.
[130] J. Chen, S. So, H. Lee, M.P. Fraser, R.F. Curl, T. Harman, F.K. Tittel, Appl. Spectrosc. 58 (2004) 243–247.
[131] H.Y. Clark, L. Corner, W. Denzer, G. Hancock, A. Hutchinson, M. Islam, R. Peverall, G.A.D. Ritchie, Chem. Phys. Lett. 39 (2004) 102–108.
[132] Z. Cao, X. Gao, L. Deng, W. Chen, Y. Yuan, W. Zhang, Z. Gong, Spectrochimica Acta A 68 (2007) 74–77.
[133] D. Richter, M. Erdelyi, R.F. Curl, F.K. Tittel, C. Oppenheimer, H.J. Duffell, M. Burton, Opt. Lasers Engrg. 37 (2002) 171–186.
[134] W. Chen, F. Cazier, F. Tittel, D. Boucher, Appl. Opt. 39 (2000) 6238–6242.
[135] E. Pollet, W. Chen, D. Boucher, in preparation.
[136] A. Khorsandi, U. Willer, L. Wondraczek, W. Schade, Appl. Opt. 43 (2004) 6481–6486.
[137] R. Barron-Jimenez, J.A. Caton, T.N. Anderson, R.P. Lucht, T. Walther, S. Roy, M.S. Brown, J.R. Gord, Appl. Phys. B 85 (2006) 185–197.
[138] L. Wondraczek, A. Khorsandi, U. Willer, G. Heide, W. Schade, G.H. Frischat, Combust. Flame 138 (2004) 30–39.
[139] A. Klingbeil, J.B. Jeffries, R.K. Hanson, Proc. Combust. Inst. 31 (2007) 807–815.
[140] A. Brun, G. Pesce, G. Rusciano, A. Sasso, Spectrochimica Acta A 58 (2002) 2481–2488.
[141] A. Brun, G. Pesce, G. Rusciano, A. Sasso, J. Mol. Spectrosc. 215 (2002) 244–250.
[142] J. Henningsen, J. Hald, Appl. Phys. B 76 (2003) 441–449.
[143] E. Poullet, W. Chen, J. Burie, D. Boucher, Int. J. IR MMW 24 (2003) 537–554.
[144] A. Vitcu, R. Ciurylo, R. Wehr, J.R. Drummond, A.D. May, Appl. Opt. 43 (2004) 4965–4971.
[145] D. Lisak, G. Rusciano, A. Sasso, J. Mol. Spectrosc. 227 (2004) 162–171.
[146] Z.S. Li, M. Rupinski, J. Zetterberg, Z.T. Alwahabi, M. Alden, Appl. Phys. B 79 (2004) 135–138.
[147] D. Halmer, S. Thelen, P. Hering, M. Mürtz, Appl. Phys. B 85 (2006) 437–443.
[148] M. Mürtz, D. Halmer, M. Horstjann, S. Thelen, P. Hering, Spectrochim. Acta A 63 (2006) 963–969.
[149] M. Erdelyi, D. Richter, F.K. Tittel, Appl. Phys. B 75 (2002) 289–295.
[150] M.E. Trudeau, P. Chen, G.A. Garcia, L.W. Hollberg, P.P. Tans, Appl. Opt. 45 (2006) 4136–4141.
[151] H. Waechter, M.W. Sigrist, Appl. Phys. B 87 (2007) 539–546.
[152] R.F. Curl, F.K. Tittel, Ann. Rep. Progr. Chem. C 98 (2002) 217–270.
[153] T. Topfer, K.P. Petrov, Y. Mine, D. Jundt, R.F. Curl, F.K. Tittel, Appl. Opt. 36 (1997) 8042–8049.
[154] M. Takahashi, S. Ohara, T. Tezuka, H. Ashizawa, M. Endo, S. Yamaguchi, K. Nanri, T. Fujioka, Appl. Phys. B 78 (2004) 229–233.
[155] T. Yanagawa, O. Tadanaga, K. Magari, Y. Nishida, H. Miyazawa, M. Asobe, H. Suzuki, Appl. Phys. Lett. 89 (2006) 221115.
[156] R. Bartlome, M. Baer, M.W. Sigrist, Rev. Sci. Instrum. 78 (2007) 0131101–01311106.
[157] S. Stry, S. Thelen, J. Sacher, D. Halmer, P. Hering, M. Mürtz, Appl. Phys. B 85 (2006) 365–374.

[158] P. Malara, P. Maddaloni, G. Gagliardi, P. De Natale, Opt. Express 14 (2006) 1304–1313.
[159] P. Maddaloni, P. Malara, G. Gagliardi, P. De Natale, Appl. Phys. B 85 (2006) 219–222.
[160] D. Lancaster, D. Richter, R.F. Curl, F.K. Tittel, L. Goldberg, J. Koplow, Opt. Lett. 24 (1999) 1744–1746.
[161] H.C. Chui, G.L. Woods, M.M. Fejer, E.L. Martinet, J.S. Harris, Appl. Phys. Lett. 66 (1995) 265–267.
[162] T. Umeki, M. Asobe, Y. Nishida, O. Tadanaga, K. Magari, T. Yanagawa, H. Suzuki, Opt. Lett. 32 (2007) 1129–1131.
[163] R.F. Service, Science 275 (1997) 1878.
[164] X. Wan, H. Xu, T. He, D. Lin, H. Luo, J. Appl. Phys. 93 (2003) 4766–4768.
[165] M. Raybaut, A. Godard, R. Haïdar, M. Lefebvre, P. Kupecek, P. Lemasson, E. Rosencher, Opt. Lett. 31 (2006) 220–222.
[166] D. Wasserman, S.S. Howard, C. Gmachl, A. Belyanin, D. Sivco, in: Conference on Lasers and Electro-Optics/Quantum Electronics and Laser Science Conference and Photonic Applications Systems Technologies 2007 Technical Digest, Optical Society of America, Washington, DC, 2007, JWA138.
[167] http://www.novawavetech.com.
[168] M. Asobe, Y. Nishida, O. Tadanaga, T. Yanagawa, T. Umeki, H. Suzuki, in: CLEO/Europe-IQEC 2007 Technical Digest, Postdeadline paper CD-2168.
[169] E. Takaoka, K. Kato, Jap. J. Appl. Phys. Part 1 38 (1999) 2755–2759.
[170] O. Balachninaite, L. Petraviciute, M. Maciulevicius, V. Sirutkaitis, L. Isaenko, S. Lobanov, A. Yelisseyev, J.-J. Zondy, Ultragarsas (ISSN1392-2114) 3 (2006) 7–10.
[171] W. Chen, E. Poullet, R. Bocquet, J. Burie, D. Boucher, M.W. Sigrist, J.-J. Zondy, L. Isaenko, A. Yelisseyev, S. Lobanov, in: Nonlinear Optics (OSA Topic Meetings): Materials, Fundamentals and Applications Technical Digest 2004, ISBN 1-55752–773-3, PD8-1.
[172] T. Skauli, K.L. Vodopyanov, T.J. Pinguet, A. Schober, O. Levi, L.A. Eyres, M.M. Fejer, J.S. Harris, B. Gerard, L. Becouarn, E. Lallier, G. Arisholm, Opt. Lett. 27 (2002) 628–630.
[173] I. Shoji, T. Kondo, A. Kitamoto, M. Shirane, R. Ito, J. Opt. Soc. Am. B 14 (1997) 2268–2294.
[174] O. Levi, T.J. Pinguet, T. Skauli, L.A. Eyres, K.R. Parameswaran, J.S. Harris, M.M. Fejer, T.J. Kulp, S.E. Bisson, B. Gerard, E. Lallier, L. Becouarn, Opt. Lett. 27 (2002) 2091–2093.
[175] R. Haïdar, A. Mustelier, Ph. Kepecek, E. Rosencher, R. Triboulet, Ph. Lemasson, G. Mennerat, J. Appl. Phys. 91 (2002) 2550–2552.